

This is an author-submitted to IEEE Communications Surveys and Tutorials article.

© 2021 IEEE. Personal use of this material is permitted. Permission from IEEE must be obtained for all other uses, in any current or future media, including reprinting/republishing this material for advertising or promotional purposes, creating new collective works, for resale or redistribution to servers or lists, or reuse of any copyrighted component of this work in other works.

# A Tutorial on Mathematical Modeling of Millimeter Wave and Terahertz Cellular Systems

Dmitri Moltchanov, Eduard Sopin, Vyacheslav Begishev,  
Andrey Samuylov, Yevgeni Koucheryavy, and Konstantin Samouylov

**Abstract**—Millimeter wave (mmWave) and terahertz (THz) radio access technologies (RAT) are expected to become a critical part of the future cellular ecosystem providing an abundant amount of bandwidth in areas with high traffic demands. However, extremely directional antenna radiation patterns that need to be utilized at both transmit and receive sides of a link to overcome severe path losses, dynamic blockage of propagation paths by large static and small dynamic objects, macro- and micromobility of user equipment (UE) makes provisioning of reliable service over THz/mmWave RATs an extremely complex task. This challenge is further complicated by the type of applications envisioned for these systems inherently requiring guaranteed bitrates at the air interface. This tutorial aims to introduce a versatile mathematical methodology for assessing performance reliability improvement algorithms for mmWave and THz systems. Our methodology accounts for both radio interface specifics as well as service process of sessions at mmWave/THz base stations (BS) and is capable of evaluating the performance of systems with multiconnectivity operation, resource reservation mechanisms, priorities between multiple traffic types having different service requirements. The framework is logically separated into two parts: (i) parameterization part that abstracts the specifics of deployment and radio mechanisms, and (ii) queuing part, accounting for details of the service process at mmWave/THz BSs. The modular decoupled structure of the framework allows for further extensions to advanced service mechanisms in prospective mmWave/THz cellular deployments while keeping the complexity manageable and thus making it attractive for system analysts.

## I. INTRODUCTION

As the standardization of fifth-generation (5G) New Radio (NR) technology operating in microwave and millimeter wave (mmWave) bands is over, the focus of the research community is shifting towards performance optimization of these systems for future cellular deployments [1], [2], [3]. At the same time, seeking for even more capacity at the air interface, the researchers already start to entertain the challenge of utilizing terahertz (THz) frequency band for cellular communications having tens of even hundred of GHz of consecutive bandwidth available [4], [5], [6], [7].

The utilization of mmWave and THz frequency bands promises to not only bring the extreme capacity to the air interface enabling novel bandwidth greedy applications such

as virtual reality (VR), augmented reality (AR), and holographic telepresence but to enable truly multi-service access networks delivering guarantees to applications sensitive to various parameters such as delay and throughput [8], [2]. However, the inherent properties of these bands including the need for extremely high radiation patterns at both sides of communications link to compensate for extreme path losses [9], [10], [11], blockage of propagation paths by large objects such as buildings [12], [13], [14] or small dynamic obstacles such as human bodies and vehicles [15], [16], [17], as well as macro- and micromobility of user equipment (UE) [18], [19], [20], [21] may drastically affect the performance of these technologies frequently leading to either drastic rate degradation or even outage situations. In fact, the performance of these radio access networks (RAT), tailored specifically towards service provisioning in crowded environments with extreme traffic demands, will suffer most in these conditions. To overcome these problems, novel mechanisms maintaining the advertised performance are needed. To evaluate the performance of these mechanisms system-level performance evaluation methodologies are required.

The system-level performance evaluation of cellular communications systems is conventionally performed utilizing either a purely mathematical approach or via computer simulations. As discussed in [22], [23], [24] the multi-path propagation and as well as dynamic blockage phenomena drastically affect the efficiency of simulation techniques. At the physical layer, the extreme mmWave and THz propagation sensitivity to different surfaces naturally call for ray tracing techniques for precise modeling [25], [26] inducing accuracy-complexity trade-off [27], [28]. Further, accounting for blockage requires capturing not only static scenario geometry and tracking UEs having active sessions but accounting for all of the dynamic objects in the channel, e.g., humans, vehicles. In these conditions, the utilization of mathematical frameworks may provide a viable way for the first-order assessment of the novel mechanisms improving the performance of mmWave and THz systems. In doing this, the frameworks proposed in the past for LTE systems [29], [30] have to be properly extended to account for specifics of mmWave and THz communications including highly directional antenna radiation patterns, static and dynamic blockage, atmospheric attenuation, etc. Notably, those frameworks have been developed assuming elastic traffic patterns inherently adaptive to network state and thus mainly utilized the elements of stochastic geometry [31], [32], [33]. Contrarily, mmWave and THz RATs, having extreme capacity at their disposal, are expected to primarily target

D. Moltchanov, and Y. Koucheryavy are with Tampere University, Finland. Email: firstname.lastname@tuni.fi

E. Sopin, V. Begishev, A. Samuylov, and K. Samouylov are with Peoples' RUDN University, Moscow, Russia. Email: begishev-vo@rudn.ru, {sopin-es, begishev-vo, samuylov-ak, samuylov-ke}@rudn.ru

E. Sopin and K. Samouylov are also with Institute of Informatics Problems, Federal Research Center Computer Science and Control of Russian Academy of Sciences, Moscow, Russia.

applications generating non-elastic traffic and requiring high and guaranteed bitrates at the air interface and having no or limited application layer adaptation capabilities [34], [35], [36]. Thus, the performance evaluation frameworks tailored towards mmWave and THz RATs have to take into account not only the specifics of the radio part and stochastic factors related to randomness of UE locations, but the traffic service dynamics at BSs by joining the tools of stochastic geometry and queuing theory.

The goal of this manuscript is to provide a comprehensive tutorial on mathematical performance analysis of prospective mmWave and THz deployments supporting non-elastic traffic and implementing advanced capabilities for improving service reliability at the air interface. To this aim, we first provide an exhaustive survey of analytically tractable models of various components utilized for building the modeling scenarios including deployment, propagation, antenna, blockage, micromobility, beamsearching, traffic, and service models for different system and environmental conditions. We discuss the abstraction levels and parameterization techniques as well as comment on the potential pitfalls and applicability of these models to considered RATs. Here, we also define both user-centric and system-centric performance indicators.

Then, we introduce the structure of the generic performance evaluation framework capable of simultaneously capturing radio part details of mmWave/THz systems as well as traffic service dynamics at BSs. For flexibility reasons, the contributed framework is divided into two parts: (i) queuing and (ii) radio abstraction. Specifically, the latter characterizes the type of deployment and abstracts the stochastic effects of radio channel via a separate parameterization part, i.e., UE locations, blockage, and micromobility, and represents them in the form suitable for the queuing part. The queuing part accepts the probability mass function (pmf) of the amount of requested resources by arriving sessions and the temporal intensity of the UE stage changes induced by blockage and micromobility processes and utilizes them to produce performance metrics.

The modular structure of the framework allows for the reuse of its core models for studying various mmWave and THz deployments characterized by different scenario geometry, blocker types and their mobility, antenna arrays, micromobility patterns of applications, network associations, reliability and rate improvement mechanisms, etc. In addition to the baseline model having a single traffic type, no priorities, and no reliability improvement mechanisms, we consider in detail more sophisticated traffic service processes at BSs in incremental order of complexity, including systems with resource reservation, multiconnectivity, and models with multiple UE types and priorities. Note that additional models can be built on top of these, e.g., by uniting multiconnectivity and priorities and defining additional rules to utilize the former, one could produce a model of a network segment with multiconnectivity capabilities servicing more than a single traffic type.

Our main contributions are:

- a comprehensive review of analytically tractable models utilized in system-level mathematical performance evaluation frameworks targeting mmWave and THz communications systems including deployment, propagation,

antenna, blockage, micromobility, beamsearching, traffic and service models;

- compound performance evaluation methodology tailored at evaluating user- and system-centric key performance indicators (KPI) of mmWave and THz communications systems capturing their critical specifics and consisting of two independent parts interfaced with each via a predefined set of parameters;
- detailed treatment of several cases of specific service processes at BS side (baseline, multiconnectivity, resource reservation, explicit priorities) as well as examples of parameterization of the framework.

The rest of the manuscript is organized as follows. First, in Section II we discuss the role of mmWave and THz systems in the future cellular ecosystem as well as review the recent proposals for improving their performance. Further, in Section III we introduce models of individual components of mmWave and THz communications systems. In Section IV, we specify the performance evaluation framework and consider its special cases. We parameterize the framework in Section V. Finally, conclusions are drawn in the last section.

## II. MILLIMETER WAVE AND TERAHERTZ SYSTEMS

In this section, we start by briefly reminding the specifics of mmWave and THz systems that differentiate them from 4G LTE systems operating in microwave band. Then, we discuss two challenges requiring development of new mechanisms: (i) reliable communications over mmWave/THz systems and (ii) support of multiple traffic types in these RATs.

### A. mmWave/THz RAT Specifics

In addition to large bandwidth air the air interface suitable for enabling applications characterized by high bitrates, mmWave systems operating in 30 – 100 GHz band and THz systems envisioned to first occupy the lower part of 0.3 – 3 THz band [4], bring new challenges to system designers. First of all, small wavelengths of these systems and limited penetration capabilities [37] lead to the frequent blockage situations induced by large static objects in the channel such as buildings [38], and mobile entities such as vehicles and humans [39], [40], [39].

Further, the extreme propagation losses increasing as a power function of the frequency naturally call for massive antenna arrays featuring tens and even hundreds of elements [11], [41]. These arrays will operate in a beamforming regime [42] and be capable of creating very directional radiation patterns with the half-power beamwidth (HPBW) values reaching few degrees for mmWave systems down to a fraction of degree for THz links [43], [44]. The later feature is vital for mmWave/THz communications systems not only allowing to overcome severe path losses but ensuring an almost interference free environment even for extreme deployment density of base stations (BS) [45]. However, as a side effect, these high directivities bring additional challenges. First of all, they lead to large beamforming codebooks, especially for THz systems, drastically increasing the beamsearching time. Secondly, in THz communications systems, in addition to macromobility,

micromobility manifesting itself in fast UE displacements and rotations have to be considered [46], [20], [47]. This phenomenon happening during the communications process may cause frequent misalignments of the highly-directional THz beams, resulting in fluctuations of the channel capacity and outages [48].

Finally, as opposed to previous generations of cellular systems, mmWave and THz RAT in 5G/6G systems will mostly target bandwidth-greedy new applications such as VR/AR, uncompressed video, holographic telepresence, and multimedia-rich extended reality (XR) services [49]. For such systems, not only uninterrupted network connectivity, but other quality of service (QoS) parameters such as guaranteed bitrate and latency become critical. Thus, we now proceed to discuss approaches recently proposed for improving session continuity in mmWave/THz systems.

### B. Reliable Communications and Session Continuity

The blockage events in mmWave/THz systems may lead to two principally different effects. When the signal-to-noise plus interference ratio (SINR) falls below a predefined threshold, the UE suffers from outage conditions. The outage probability depends on many system parameters including propagation conditions, receiver sensitivity, utilized power, as well as antenna arrays at both BS and UE. The effect of micromobility is similar in nature and is heavily affected by the type of application utilizing the wireless channel [20]. To ensure uninterrupted service in mmWave/THz deployments, one may utilize multiconnectivity operation standardized by 3GPP [50]. According to it, UE is capable of maintaining multiple connections with the nearest BSs within the same RAT. These connections can be utilized for data transmission simultaneously. Even when only one of these connections may be utilized at a time, the packet flow can be rerouted to the backup connection should the current link experience outage conditions. However, the efficient use of this technique inherently requires dense deployments that may not be available at early phases of mmWave/THz systems rollouts.

Vendors and standardization bodies also consider the support of multiple RATs at the UE via multi-band multiconnectivity option [51]. This approach addresses outage problem by timely rerouting traffic to the backup connection when the currently active link becomes unusable. However, the inherent rate mismatch between RATs utilized in future 5G/6G deployments, especially, between mmWave/THz and LTE interfaces, may render this capability useless in practical use cases. Moreover, recall that the outage events caused by micromobility and blockage by small dynamic objects such as human or vehicle bodies are characterized by rather short duration and high frequency [52], [19], [24]. Thus, the resulting traffic that needs to be supported at lower rate interfaces is expected to be bursty in nature. These occasional traffic spikes caused by high bitrate sessions temporarily offloaded onto lower rate interface may negatively affect the service performance of other sessions and also lead to inefficient resource utilization of the corresponding BSs. As a result, traffic protection strategies might be required.

The blockage may not lead to an outage when the SINR still remains higher than the one associated with the lowest

possible MCS. In this case, even though the connection is not lost the amount of resources required to maintain the required bitrate increases drastically. To address this case, the authors in [53] suggested the use of the resource reservation technique. According to it, a fraction of BS resources is reserved for sessions that are accepted for service ensuring that there is a surplus of resources for them when their state changes from non-blocked to blocked. This approach is fully localized at the BS and thus can be utilized at the early rollouts of mmWave/THz RATs when the network density is insufficient to efficiently utilize multiconnectivity operation. Furthermore, it does not require maintaining active connections to more than a single BS reducing the complexity of the UE implementation. However, by joining this technique with multiconnectivity one may attain additional gain in terms of session service performance [54].

### C. Traffic Types Coexistence

Modern cellular systems are being developed having multiple types of traffic in mind with drastically different service requirements. As an example, the NR radio interface is expected to support at least two traffic types [55], [51]. At one extreme, there is enhanced mobile broadband (eMBB) service which is an extension of the broadband access provided in 4G LTE technology having similar service requirements. In industrial automation scenarios, 5G NR is also expected to enable specific services, such as positioning, clock synchronization, joint tasks execution. All these applications are characterized by extreme latency and reliability requirements and need to be supported via ultra-reliable low-latency (URLLC) service. This implies that future BSs need to support a mixture of traffic with drastically different service requirements at the air interface. Mechanisms for supporting eMBB or URLLC in isolation are current the focus of ongoing studies, see, e.g., [56], [53], [57] for eMBB and [58], [59], [60] for URLLC. Their joint support, however, requires advanced techniques at BS side.

There have been two principally different approaches for enabling the coexistence of eMBB and URLLC at the air interface. The first one implies the use of smart scheduling techniques. This approach has been taken in [61] to formalize the optimization problem of joint scheduling of these services. While discussing their results, the authors concluded that the major impact is produced by the minimum scheduling interval utilized by the technology in question. To alleviate this limitation, several studies suggested the use of non-orthogonal multiple access (NOMA) technique, e.g., [62], [63], [64]. According to NOMA, properly encoded URLLC transmissions can be superimposed on top of already scheduled eMBB traffic and the message content can be restored at the receiving end. While this approach may indeed drastically reduce the latency, the reliability of communications still remain a challenging problem. On top of this, the intended UEs need to be always awake to receive the intended transmissions.

An alternative approach is based on explicit resource allocation and prioritization techniques. When the minimum scheduling interval allows for satisfying latency constraints,

one may utilize, e.g., network slicing techniques at the air interface to explicitly allocate a part of resources to URLLC traffic [65], [66], [67]. However, as a load of URLLC traffic may not be known in advance this approach may result in inefficient use of resources. A viable alternative is to utilize priorities between traffic flows as illustrated in [68], [69]. Compared to the resource reservation technique, this approach does not suffer from resource utilization problem but may lead to reduced service performance of eMBB flows.

### III. MODELS OF INDIVIDUAL ELEMENTS

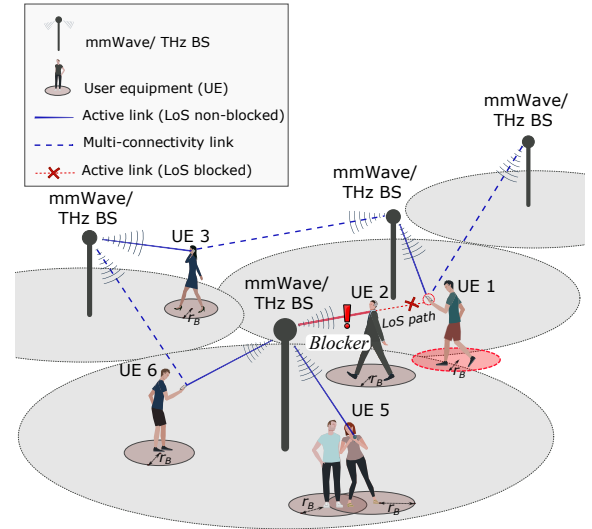
In this section, we survey analytically tractable models of various components that can be utilized as building blocks for specifying the prospective mmWave and THz deployment scenarios. These include BS and UE locations, propagation, antenna, blockage, micromobility, beamsearching models. For each model, we discuss the level of abstraction, parameterization and comment on its applicability to considered RATs.

#### A. Deployment Models

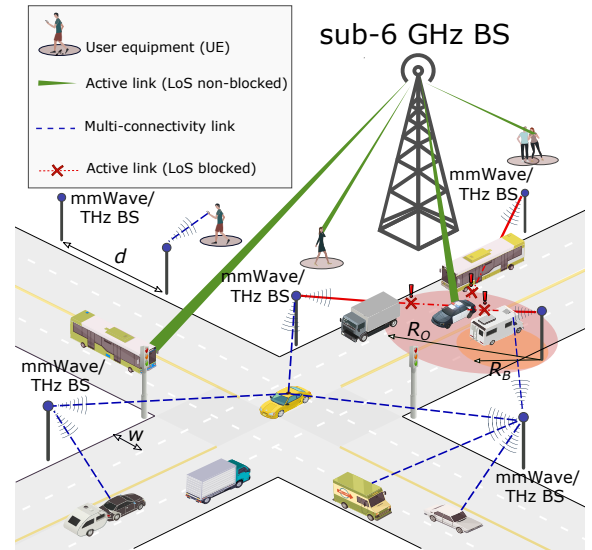
The choice of the deployment model, i.e., indoor/outdoor as well as BS and UE locations, for mmWave and THz systems is a more critical question as compared to microwave ones. The rationale is that now scenario geometry that involves not only deployment premises but the type of the surrounding objects that may cause blockage starts to play an important role in systems performance. Particularly, in addition to the effects of indoor and outdoor propagation the relative positioning of these objects affects the tractability of considered deployments. Furthermore, the directionality of antenna radiation patterns coupled with inherent multipath propagation of mmWave/THz bands forces researchers to switch from conventional two-dimensional (2D) models to more comprehensive three-dimensional (3D) ones. Finally, in addition to UE and BS locations, one should also need to specify blocker types, locations and/or their mobility.

1) *Purely Random Deployments*: Following the studies of microwave LTE systems [30], [29], the early works on mmWave and THz systems performance, e.g., [70], [71], [45], assumed purely stochastic 2D deployments, where BSs, UEs, and blockers are assumed to follow certain stochastic processes in  $\mathbb{R}^2$ , see Fig. 1(a). Here, active UEs are often characterized as a separate process or included (as a fraction of) in the specification of blockers representing humans. Often, a homogeneous point Point process (PPP) is utilized for tractability reasons. Indeed, the geometric distances between points in PPP are readily available [72], the coverage area of a BS can be roughly approximated by Voronoi diagrams [32], while the distance between BS and UE can be found assuming circle approximation of Voronoi cells.

The rationale behind the use of purely stochastic deployments is that the locations of BSs may not follow regularity assumption (i.e., cellular deployments) and possess a certain degree of randomness as discussed in [73]. Furthermore, UE may indeed be naturally randomly distributed within the cell coverage area. Finally, the use of 2D planar deployments is warranted when antenna radiation patterns are not extremely



(a) Outdoor random deployment



(b) Outdoor semi-regular deployments

Fig. 1. Illustration of different deployment environments.

directional in the vertical dimension. Such purely random 2D deployments may still be relevant for mmWave systems in outdoor open space conditions, where the coverage of a single BS is relatively large reaching few hundreds of meters, such as squares, parks, suburbs, etc.

Recently, extensions of these deployment models to 3D open space environments have been provided [74], [75], [76], [77] in context of UAV communications. Here, in addition to the planar deployment assumption, one has to characterize vertical dimension by supplying BS, UE and blocker height distributions. Assuming analytically convenient distributions such as exponential or uniform mathematically tractable models can be provided.

2) *Semi-Regular Deployments*: As mmWave and THz BSs are characterized by much smaller coverage areas compared to sub-6 GHz BS, the impact of scenario geometry and type of the objects in the channel is expected to be profound. This concerns both outdoor and indoor environments. First,

in urban street deployments, locations of BSs are no longer stochastic and likely follow regular deployment along the street, e.g., BSs are mounted on lampposts or building walls [78], [79], [23], UE are also naturally located along the sidewalks and crossroads. In addition to humans blocking the propagation paths, vehicles moving along straight trajectories may contribute to the blockage process in mmWave and THz systems [80], [81], [82], [83], see Fig. 1(b). In city squares, BSs may also be installed along the perimeter [54], [84]. Finally, the dimensions of blockers, e.g., vehicles, can be comparable to the communications distances and thus one may need to take into account detailed blockers geometry. The latter is also critical for indoor THz system deployments [85], [86].

The abovementioned specifics naturally lead to semi-regular environments with stochastic factors interrelated with deterministic ones. Particularly, the conventional Poisson process may not be applicable for modeling vehicle and pedestrian locations due to potential overlapping between adjacent objects requiring the utilization of hardcore processes. The potential specific locations of BS, i.e., building corners, walls, lampposts, crossroad centers lead to different performance results [87]. The analysis is further complicated by 3D specifics including heights of blockers, BS and UEs. As a result, the use of stochastic geometry for addressing radio part performance, although feasible, is usually more complicated and tedious as compared to purely stochastic deployments as discussed in [87], [88], [89].

## B. Propagation Models

Generally, there are two types of propagation models for mmWave and THz communications system: (i) ray-tracing models and (ii) models based on fitting of measurements data. Although the former may precisely account for details of the propagation environment leading to very accurate models, they, by design, cannot be utilized in mathematical modeling of communications systems. However, these models as well as empirical experiments allow to formulate empirical models. These models are based on the fitting experimental data to mathematical expressions and can further be classified into two large groups: (i) ‘‘averaged’’ models and (ii) 3D multi-path cluster-based models.

1) *Averaged Models*: The SINR at the UE is written as

$$S(y) = \frac{P_A G_A G_U L(y)}{N_0 + I}, \quad (1)$$

where  $y$  is the 3D distance between BS and UE,  $P_A$  is the transmit power at BS,  $G_A$  and  $G_U$  are the antenna gains at the BS and the UE, respectively,  $N_0$  is the thermal noise at the UE,  $L(y)$  is the path loss, and  $I$  is the interference.

Note that propagation  $L(y)$  and interference  $I$  components in (1) are often random variables (RV). In (1), one may also account for fast fading and shadow fading phenomena via additional RVs with exponential and Normal distributions, respectively, [90]. To simplify the model, the shadow fading effect is often accounted for by margins,  $M_{S,1}$  and  $M_{S,2}$  for the LoS non-blocked. These margins are specified in [90].

To define the path loss,  $L(y)$ , for mmWave systems one may utilize the models defined in [90]. Particularly, the urban-micro (UMi) path loss is dB scale is readily given by

$$L_{dB}(y) = \begin{cases} 32.4 + 21 \log_{10} y + 20 \log_{10} f_c, & \text{non-bl.,} \\ 32.4 + 31.9 \log_{10} y + 20 \log_{10} f_c, & \text{blocked,} \end{cases} \quad (2)$$

where  $f_c$  is the carrier measured in GHz. The UMi path loss model for the 140 GHz band has been introduced in [91] while [86] reports indoor-hall (InH) model for the same frequency.

The path loss defined in (2) can also be converted to the linear scale by utilizing the generic representation  $A_i y^{-\zeta_i}$ , where  $A_i$ ,  $\zeta_i$ ,  $i = 1, 2$ , are the propagation coefficients corresponding to LoS non-blocked ( $i = 1$ ) and blocked ( $i = 2$ ) conditions, i.e.,

$$A = A_1 = A_2 = 10^{2 \log_{10} f_c + 3.24}, \quad \zeta_1 = 2.1, \quad \zeta_2 = 3.19. \quad (3)$$

Now, the SINR at the UE can then be rewritten as

$$S(y) = \frac{P_A G_A G_U}{A(N_0 + I)} [y^{-\zeta_1} [1 - p_B(y)] + y^{-\zeta_2} p_B(y)], \quad (4)$$

where  $p_B(y)$  is the blockage probability [40]

$$p_B(y) = 1 - \exp^{-2\lambda_B r_B \left[ \sqrt{y^2 - (h_A - h_U)^2} \frac{h_B - h_U}{h_A - h_U} + r_B \right]}, \quad (5)$$

where  $\lambda_B$  is the blockers density,  $h_B$  and  $r_B$  are the blockers’ height and radius,  $h_U$  is the UE height,  $h_U \geq h_B$ ,  $h_A$  is the BS height,  $y$  is the 3D distance between UE and BS.

Finally, introducing the coefficient

$$C = P_A G_A G_U / A, \quad (6)$$

the SINR at UE can be compactly written as

$$S(y) = \frac{C}{N_0 + I} [y^{-\zeta_1} [1 - p_B(y)] + y^{-\zeta_2} p_B(y)]. \quad (7)$$

2) *Absorption Losses in mmWave and THz Bands*: The unique property of the mmWave and THz channels is the atmospheric (molecular) absorption [92], [93]. In the mmWave band, absorption is mostly due to the oxygen molecules while in the THz band it is mainly caused by the atmospheric water vapor [94]. These losses may induce frequency selectivity in the channel characteristics. With absorption losses accounted for, the SINR at the UE takes the following form

$$S(y) = \frac{P_A G_A G_U L(y) L_A(y)}{N_0 + I}, \quad (8)$$

where the additional factor  $L_A(y)$  represents absorption losses. Following [92], the absorption loss is defined as

$$L_A(y) = 1/\tau(y), \quad (9)$$

where  $\tau(y)$  is the medium transmittance described by the Beer-Lambert-Bouguer law. The latter is related to the frequency dependent absorption coefficient  $K(f)$  as  $\tau(y) \approx e^{-K(f)y}$ . The values of  $K(f)$  can be obtained from [94] as described in detail in [92], [93].

Note that in mmWave band absorption losses are only non-negligible in the 60 GHz band that is utilized for WLAN systems. In the THz band, there are so-called transparency windows [95], where the impact of these losses is negligible

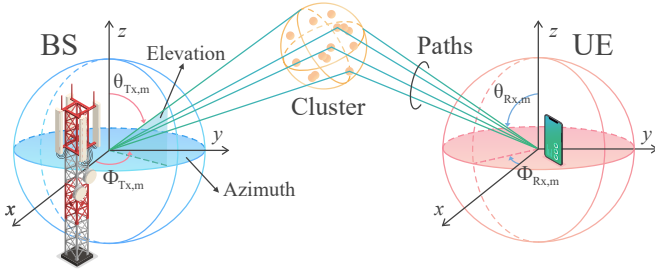


Fig. 2. Illustration of the 3D cluster-based propagation model.

as well. Finally, the absorption phenomena may also lead to the molecular noise theoretically predicted in [92]. The theoretical model for molecular noise has been proposed in [96]. However, recent measurements [97] did not reveal any noticeable impact of molecular noise phenomenon.

3) *Cluster-based Models*: MmWave and THz channels are inherently characterized by multi-path nature. To this aim, 3GPP standardized 3D channel model for 6 – 100 GHz band in [90]. The structure of the model, see Fig. 2, is essentially similar to the LTE 3D model specified in [98], with enhancements inherent to mmWave propagation such as a blockage. According to it, the received power consists of energy coming from LoS and reflected paths. Here, the term cluster is interpreted as a surface potentially leading to the reflection of propagating rays. Taking the number of clusters in the range of 5 – 20 as an input, this model relates the specifics of the propagation environment to a set of parameters that include: (i) zenith of departure and arrival (ZoD/ZoA), (ii) azimuth of departure and arrival (AoD/AoA), (iii) number of rays (paths) in a cluster, (iv) cluster delay, (v) power fraction of a cluster, and (vi) other parameters such as Ricean K-factor.

The 3GPP 3D cluster model has an explicit algorithmic structure providing no closed-form expressions for the above-mentioned parameters. However, the authors in [99] provided analytical approximations for selected parameters required for the use of this model in mathematical analysis of mmWave systems. Particularly, they have shown that the power of a cluster follows Log-Normal distribution while AoA and ZoA can be approximated by Laplace distribution, i.e.,

$$f_{\theta_i}(y; x) = \frac{1}{2a_{i,2}(x)} e^{-\frac{|y - a_{i,1}(x)|}{a_{i,2}(x)}}, \quad i = 1, 2, \dots, W,$$

$$f_{P_{S,i}}(y; x) = \frac{1}{ya_{i,4}\sqrt{2\pi}} e^{-\frac{(\ln y - a_{i,3})^2}{2a_{i,4}^2}}, \quad i = 1, 2, \dots, \quad (10)$$

where  $a_{i,1}(x)$ ,  $a_{i,2}(x)$ ,  $a_{i,3}(x)$ , and  $a_{i,4}(x)$ ,  $i = 1, 2, \dots, W$ , are the parameters estimated from statistical data, see [99] for details. It has also been shown in [99] that  $a_{i,1}(x)$  are independent of the cluster number  $i$  and only depend on the separation distance  $x$ . Further, the mean of ZoA for all clusters coincides with the constant ZoA of the LoS cluster. In its turn,  $a_{i,2}(x)$ ,  $a_{i,3}(x)$ , and  $a_{i,4}(x)$  are independent of the distance and only depend on the cluster number, see [99]. The utilization of the model is demonstrated in [17], [99], [54].

As of now, 3D cluster model parameters are only available for mmWave bands for outdoor deployment conditions [90].

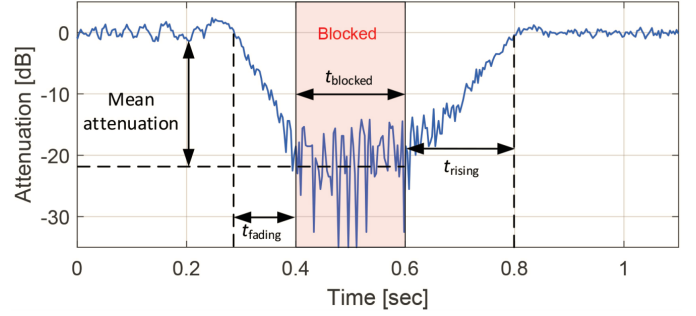


Fig. 3. Typical blockage profile at 60 GHz, reproduced from [112].

For other environments, such as vehicle-to-vehicle (V2V) and vehicle-to-infrastructure (V2I) communications exhaustive data for parameterization have been recently reported [80], [100]. Despite similar structure is expected to be retained by THz models as well, only a few comprehensive measurements studies are available to date that can be used to infer channel parameters, see e.g. [83] for V2V, [101] for the train to infrastructure links, as well [102] for a static kiosk application.

4) *Other Types of Impairments*: In addition to the path loss as well as blockage considered in the subsequent sections, meteorological conditions such as rain [104], [105], [106], fog [107], [108], snow [109] and foliage [110], [111] may provide additional impairments on mmWave and THz propagation summarized in Table I. As one may observe, foliage produces the most significant impact resulting in up to 2 dB/m of additional degradation. On the other hand, the impact of snow, fog, and cloud is insignificant, i.e., less than 1 dB/km. Finally, up to 10 dB/km of signal degradation is induced by rain. The impact of these environmental conditions is expected to be higher for the THz band. These values can be utilized as an additional constant in path loss models defined above.

### C. Static and Dynamic Blockage Models

Blockage caused by dynamic objects in the channel is an inherent property of mmWave and THz systems. Depending on the induced attenuation on top of the path loss, the blockage may or may not lead to outage conditions. In the latter case, the communications may still be possible at much reduced modulation and coding scheme (MCS). In the former case, depending on outage duration, application layer connectivity may or may not be interrupted. Thus, to comprehensively characterize it for performance evaluation studies one needs to provide: (i) attenuation values induced by different objects in the channel and (ii) blockage intervals under different types of UE and blockers and their mobilities.

TABLE I  
IMPACT OF ENVIRONMENTAL CONDITIONS ON MMWAVE PROPAGATION,  
REPRODUCED FROM [103]

Type	Value	Measurements
Rain	50 mm/hr	<10 GHz: 1-6 dB/km, >10 GHz: 10 dB/km
Fog	0.5g/m <sup>3</sup>	50 GHz: 0.16 dB/km, 81 GHz: 0.35 dB/km
Snow	700g/m	35-135 GHz: 0.2-1 dB/km
Foliage	0.5m <sup>2</sup> /m <sup>3</sup>	28.8, 57 GHz: 1.3-2.0 dB/m, 73 GHz: 0.4 dB/m

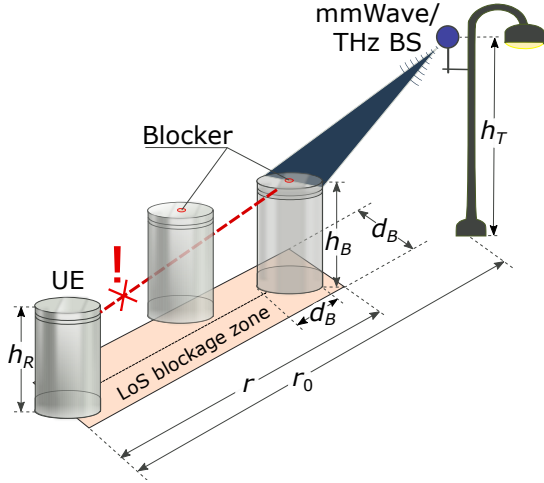


Fig. 4. Illustration of the LoS blockage zone.

The dynamic human body blockage introduces additional uncertainty in the channel resulting in drastic fluctuations in the received signal. An illustration of the typical measured path loss experienced as a result of human body blockage by UE in the 60 GHz band is shown in Fig. 3. The absolute values of blockage induced attenuation heavily depend on the type of blockers. For human body blockage in mmWave band values of losses in the range of 15–25 dB have been reported [113], [16], [114]. For THz band these losses are expected to reach 40 dB [115]. Blockage by vehicles at 300 GHz heavily depends on the vehicle type and geometry and reported to be from 20 dB at the front-shield glass level up to 50 dB at the engine level. They are considerably higher than those for mmWave band. Particularly, at 60 GHz, 5 dB–30 dB blockage losses have been reported. Note that the values of blockage losses also depend on the vehicle size and the number of them between communicating entities [116]. For 28 GHz, the authors in [80], [81], [117] also report the following height-dependent vehicle blockage losses: 11 dB–12.2 dB for 1.7 m, 13.3 dB for 1.5 m, and 30 dB–40 dB for 0.6 m.

The fading and recovery phases highlighted in Fig. 3 are reported to be on the scale from tens to a couple of hundreds of milliseconds [112], [16], [114]. Similar observations have been made recently for THz links [115]. In mathematical modeling, these phases are often omitted assuming that fading and recovery phases are negligibly small compared to the blockage duration. The blockage models utilized in performance evaluation frameworks attempt to predict the probability of blockage and blockage duration that can be caused by multiple blockers occluding the propagation paths between UE and BS.

1) *Static Human Body Blockage Models*: Most of the static blockage models proposed in the literature, e.g., [118], [40], assume the following model. Consider the static case of stationary UE in  $\mathbb{R}^2$  located in stationary homogeneous PPP of blockers with intensity  $\lambda_B$  considered in [40]. Assume that UE is located at a 2D distance  $r_0$  from the BS. UE and BS are located at heights  $h_T$  and  $h_R$ , respectively. Human bodies are represented by cylinders with constant height  $h_B$  and base diameter  $d_B = 2r_B$ . In the considered scenario, one may introduce the so-called “LoS blockage zone” of rectangular

shape with sides  $2r_B$  and  $r$  as shown in Fig. 4. Observe that the LoS is blocked when a center of at least one blocker is located inside this zone. Utilizing the void probability of the Poisson process the LoS blockage probability immediately follows

$$p_B(x) = 1 - e^{-2\lambda_B r_B \left[ r_0 \frac{h_B - h_R}{h_T - h_R} + r_B \right]}. \quad (11)$$

Analyzing (11) one may deduce that the blockage probability increases exponentially as a function of blockers density. The heights of UE and BS also affect the final values. Note that this model can be utilized in those cases when UE and blockers are stationary or to predict the time-averaged behavior of mobile blockers in the mobile field of blockers. However, in performance evaluation frameworks addressing session continuity parameters, one needs to characterize blocked and non-blocked times explicitly as discussed below.

2) *Mobile UE and Static Blockers*: Consider the case when UE moves according to the uniform rectilinear pattern in a static homogeneous PPP of blockers considered in [119]. In this case, in addition to the fraction of time UE spends in blockage, one is also interested in conditional blockage probabilities of UE at  $M$  given a certain state at  $O$ , see Fig. 5. To capture dependence between links states one may utilize conditional probabilities defined as  $p_{ij} \mathbb{P}\{\text{at } M \text{ LoS blocked/non-blocked given that LoS at } O \text{ is blocked/non-blocked}\}$ . These probabilities can be formed in a matrix as

$$P = \begin{pmatrix} p_{00} & p_{01} \\ p_{10} & p_{11} \end{pmatrix} \quad (12)$$

where states 0 and 1 reflect the non-blocked and blocked states. In general, these probabilities are a function of: (i) distance from  $O$  to  $P$ ,  $r_0$ , (ii) distance from  $O$  to  $M$ ,  $d$ , (iii) angle  $\angle POM$ , see Fig. 5, (iv) blockers density  $\lambda_A$ , (v) heights of UE and BS at  $P$ ,  $O$ , and  $M$ ,  $h_C$ . Observing that

$$p_{00} = 1 - p_{01}, \quad p_{10} = 1 - p_{11}, \quad (13)$$

one needs  $p_{00}$  and  $p_{11}$  to fully parameterize (12).

The illustration of the model is shown in Fig. 5, where rectangles represent the areas affecting the blockage of  $PO$  and  $PM$  links. Their width and length are determined by the blockers diameter  $d_B = 2r_B$  and the link lengths  $PO$  and  $PM$ . The intersection area of these rectangles visually represents the correlation between link states. Particularly, this zone can be further divided into sub-zones that affect it differently. More specifically, zone 4 is further split into two smaller zones,  $4a$  and  $4b$ , representing the area on the right and left sides, respectively, along with the  $PU$  line of intersection of two planes. Observe that zone 1 can be excluded as it is fairly small for any potential geometry. Zones 2 and 3 affect LoS state at  $O$  and  $M$ , respectively. Furthermore, LoS state at both  $O$  and  $P$  is simultaneously affected by zones  $4a$  and  $4b$ . By using these observations, the probability  $p_{00}$  is obtained as

$$p_{00} = P[nB \text{ at } M | nB \text{ at } O] = \frac{P[nB \text{ at } M \cap nB \text{ at } O]}{P[nB \text{ at } O]}, \quad (14)$$

where  $nB$  and  $B$  denote LoS non-blocked and blocked states. Once  $p_{ij}$  are determined, conditional and unconditional cumulative distribution function (CDF) and probability density function (pdf) of time spent in blocked and non-blocked states can be determined as shown in [39].





all UEs located within the same grid cell. As a result, in this model, two nearby UEs may still have completely independent conditions. Furthermore, the grid dimensions are chosen rather arbitrarily. Finally, according to the last method, *method of geometrical cluster locations*, small-scale 3D cluster model parameters such as cluster delays, AoD and AoA, ZoD and ZoA are generated in a correlated manner. It is critical that all the considered models the parameters affecting the correlation distance are chosen arbitrarily without direction relation to the blockers density and geometry.

There have been only a few attempts other than those standardized by 3GPP to capture spatial correlation caused by mobile objects including vehicles and human crowds. The study in [123] measured the UE blockage probability to multiple BSs and reported correlation states between multiple links. The authors in [124] proposed a mathematical model to derive blockage probability to multiple BS simultaneously. Note that their model is principally similar to the one described above for the case of mobile UE and static blockers. Based on the results of [119] the authors in [39] provided a model ensuring spatial consistency that does not require the correlation distance to be known in advance. They revealed that the correlation distance in mmWave band for a wide range of blockers density is limited to just a few meters.

#### D. Blockage by Large Static Objects

In addition to blockage by small dynamic objects such as humans or vehicles, propagation paths in mmWave and THz systems can be blocked by large static objects such as buildings [125], [126], [127], [128], see Fig. 7. To distinguish from dynamic blockage, in 3GPP terminology, blockage by large static objects is referred to as non-LoS conditions.

There have been several models proposed in the past to model building blockage phenomena. The critical part of these models affecting their analytical tractability is the choice of the city deployment. Particularly, in [125] the authors propose a random shape theory to model irregular deployment of buildings. The buildings are represented as rectangles with random sizes having their centers forming a homogeneous PPP. The proposed approach suits well for those deployments, where building locations are purely stochastic. The authors in [128] formalized the so-called “ball” model, where there

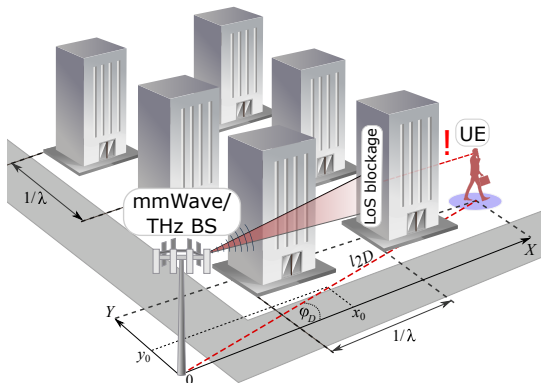


Fig. 7. LoS blockage probability by buildings.

is always LoS in a certain circularly shaped area around UE. In addition to the stochastic city deployments, studies addressing the regular city grids has also been performed. In [127] the city grid has been captured using the Manhattan Poisson line process (MPLP), where the lines represent the streets. In general, analysis of LoS probability in semi-regular deployments is more involved compared to stochastic ones.

The regular city grid deployment has also been considered by standardization bodies including both ITU-R and 3GPP. Specifically, ITU-R P.1410 considers the frequency band 20 – 50 GHz and presents LoS probability in the following form

$$P_{LoS}^{ITU} = \prod_{n=0}^m \left[ 1 - \exp \left[ \frac{[h_T - \frac{(n+\frac{1}{2})(h_T-h_R)}{m+1}]^2}{2\gamma^2} \right] \right], \quad (17)$$

where  $m = \lfloor r\sqrt{\alpha\beta} \rfloor - 1$  is the mean number of buildings in between UE and BS,  $r$  is the 2D distance measured in kilometers,  $h_T$  and  $h_U$  and are BS and UE heights. The parameters  $\alpha$ ,  $\beta$ , and  $\gamma$  are the input model parameters representing the deployment specifics including building dimensions, density, and height. One of the limitations of the model is that it does not capture 2D spatial locations of buildings concentrating on buildings locations on a LoS projection between UAV and BS to  $\mathbb{R}^2$ . Although this model accounts for different mean heights of BS and UE, it does not capture their height distributions as well as LoS AoD.

In TR 36.777 3GPP has also proposed a large-scale LoS blockage model. This model differentiates between deployment types providing the separate solutions for them. The structure of the model is also unique for different heights of BS and UE. For UMi environment with appropriate heights of BS and UE, the LoS blockage probability is

$$P_{LoS}^{3GPP} = \begin{cases} 1, & l_{2D} \leq d, \\ \frac{d}{l_{2D}} + \left[ 1 - \frac{d}{l_{2D}} \right] \exp \left[ \frac{-l_{2D}}{p_1} \right], & l_{2D} > d, \end{cases} \quad (18)$$

where the variables  $p_1$  and  $d$  are defined as

$$p_1 = 233.98 \log_{10}(h_R) - 0.95 \\ d = \max(294.05 \log_{10}(h_R) - 432.94, 18). \quad (19)$$

The generic structure of the 3GPP model makes it complicated to apply it for the specific city deployment with unique dimensions. In general, the 3GPP model also requires careful choice of parameters to assess the performance related to the specific deployment.

The ITU-R model has been extended to 3D deployments by the authors in [126]. Although the model has been originally developed for UAV LoS blockage it can also be applied to the case of BS to terrestrial UE communications. Following their study, the LoS probability is provided by, see Fig. 7,

$$P_{LoS}(l_{2D}, \phi_D) = \\ = F_{H_B}(h_m^0) \exp \left( - \lambda \int_{x_0}^{l_x} \left[ 1 - F_{H_B}(h_m^x(x)) \right] dx - \right. \\ \left. - \lambda \int_{y_0}^{l_y} \left[ 1 - F_{H_B}(h_m^y(y)) \right] dy \right), \quad (21)$$

$$f_{T_A}(t) = \frac{e^{-\frac{(\log(t)-\mu_x)^2}{2\sigma_x^2}}}{\sigma_x} \left[ 2 - \operatorname{erfc} \left( \frac{\mu_y - \log(t)}{\sqrt{2}\sigma_y} \right) \right] + \frac{e^{-\frac{(\log(t)-\mu_y)^2}{2\sigma_y^2}}}{\sigma_y} \left[ 2 - \operatorname{erfc} \left( \frac{\mu_x - \log(t)}{\sqrt{2}\sigma_x} \right) \right] + \frac{e^{-\frac{(\log(t)-\mu_\phi)^2}{2\sigma_\phi^2}}}{\sigma_\phi} \left[ 2 - \operatorname{erfc} \left( \frac{\mu_\theta - \log(t)}{\sqrt{2}\sigma_\theta} \right) \right] + \frac{e^{-\frac{(\log(t)-\mu_\theta)^2}{2\sigma_\theta^2}}}{\sigma_\theta} \left[ 2 - \operatorname{erfc} \left( \frac{\mu_\phi - \log(t)}{\sqrt{2}\sigma_\phi} \right) \right]}{4\sqrt{2\pi}t \left[ 1 - \frac{1}{2}\operatorname{erfc} \left( \frac{\mu_\phi - \log(t)}{\sqrt{2}\sigma_\phi} \right) + \frac{1}{2}\operatorname{erfc} \left( \frac{\mu_\theta - \log(t)}{\sqrt{2}\sigma_\theta} \right) \right]^{-1} \cdot 4\sqrt{2\pi}t \left[ 1 - \frac{1}{2}\operatorname{erfc} \left( \frac{\mu_x - \log(t)}{\sqrt{2}\sigma_x} \right) + \frac{1}{2}\operatorname{erfc} \left( \frac{\mu_y - \log(t)}{\sqrt{2}\sigma_y} \right) \right]^{-1}}. \quad (20)$$

where  $F_{H_B}(x)$  is the CDF of building block height,  $F_{H_B}(h_m^0)$  is the probability that the height of the first building along the LoS path is lower than LoS height,  $h_m^0$ ,  $F_{H_B}(h_m^x(x))$  and  $F_{H_B}(h_m^y(y))$  are the probabilities that the sides perpendicular to the  $Ox$  and  $Oy$  axes are lower than the LoS heights,  $h_m^x(x)$  and  $h_m^y(y)$ , at the point of their intersection, respectively. The authors have also derived closed-form solutions for uniformly, exponentially and Rayleigh distributed building heights.

The large-scale static and small-scale dynamic blockage models need to be utilized together for performance assessment of mmWave and THz deployments. This can be done similarly to [129], where the authors determined zones corresponding to exhaustive superposition of nLoS and blockage states, i.e., (LoS,blocked), (LoS,non-blocked), (nLoS,blocked), (nLoS, non-blocked). Further, the performance of UEs located in these zones can be analyzed separately and then combined by weighting with probabilities of UE being located in these zones. We also note that due to inherent limitations on the communications range, blockage by buildings may not be relevant for THz cellular systems.

### E. UE Micromobility Models

In addition to static and dynamic blockage affecting the performance of users, for mmWave/THz systems micromobility, manifesting itself in fast UE displacements and rotations, have to be considered [46], [20], [47], see Fig. 8. This phenomenon happening during the communications process may cause frequent misalignments of the highly-directional THz beams, resulting in fluctuations of the channel capacity

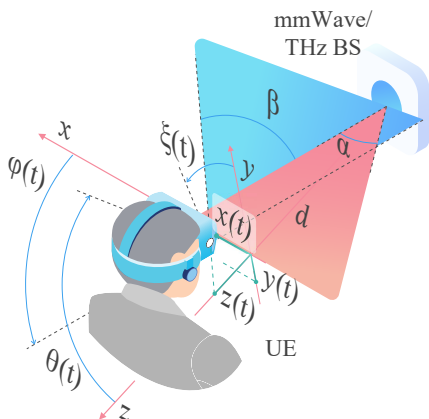


Fig. 8. Illustration of the UE micromobility process.

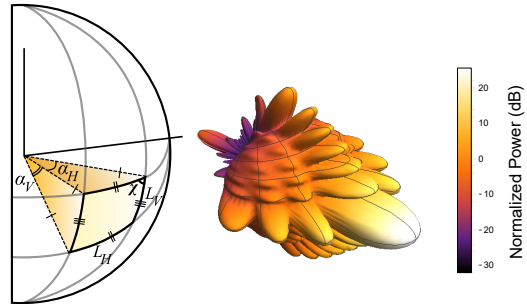


Fig. 9. Illustration of the 3D antenna radiation pattern models.

and outage events [48]. The preliminary studies indicate that the outage in THz systems might happen at much smaller timescales compared to blockage, i.e., on the order of few tens of milliseconds [20], [19]. This property challenges the development of efficient beamtracking algorithms that are critical for mmWave and THz communications.

To date, only a few micromobility models have been proposed. The authors in [19] first demonstrated that small displacements over  $Oz$  axis as well as roll (longitudinal axis) motion do not affect link performance. They further utilized the decomposition technique by modeling motion over Cartesian  $Ox$  and  $Oy$  axes as well as rotations over vertical (yaw) and transverse (pitch) axes,  $\phi(t)$  and  $\theta(t)$ , see Fig. 8, by mutually independent Brownian motions. The authors revealed that the pdf of time to outage due to beam misalignment  $f_{T_A}(t)$  follows (20), where  $\operatorname{erfc}(\cdot)$  is the complementary error function,  $\mu_{(\cdot)}$  and  $\sigma_{(\cdot)}$  are the parameters of the corresponding displacement and rotation components that can be estimated from the empirical data.

We specifically note that the model in (20) represents only the essentials of the UE micromobility process as it does not capture potential dependence between movements, distance-dependent velocity and drift to the origin. Observing that micromobility may lead to outage conditions, for performance evaluation purposes one needs to jointly represent the blockage and micromobility processes. This can be done by, e.g., superposing blockage process on top of micromobility process or abstracting both processes by a certain stochastic process with the joint intensity of link interruptions.

### F. Antenna Array Models

The ability to accurately capture essential features of BS and UE antenna radiation patterns is critical for performance

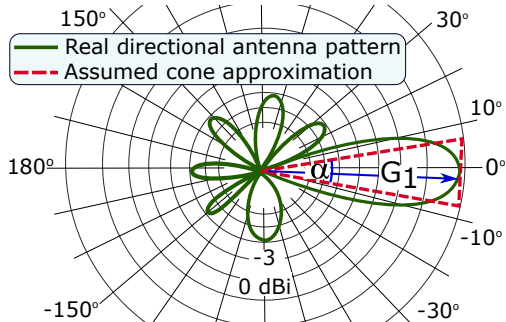
analysis of mmWave and THz communications systems. A very detailed model based on correlated superposition of individual antenna elements can be produced by utilizing the 3GPP procedure specified in 3GPP TR 37.977, see Fig. 9. However, this model is not analytically tractable. As a result, various approximations are utilized in the literature. Below, we consider typical models utilized for these purposes.

1) *2D Cone and Cone-Plus-Sphere Models*: The simplest models capturing the essential feature of mmWave and THz systems is the so-called 2D cone model and the extended 2D cone-plus-sphere model, see Fig. 10, considered in many early studies of mmWave and THz systems [45], [130], [131], [132], [133], [134]. According to the first model, illustrated in Fig. 10(a), a cone-shaped pattern parameterized by a single parameter  $\alpha$  – HPBW of the main lobe – is utilized for representing the antenna radiation pattern. The second model, shown in Fig. 10(b), attempts to account for imperfections of antenna design by modeling back and side lobes as a sphere around UE. To fully parameterize the former model one needs to determine the antenna gain  $G$  as a function of the directivity angle  $\alpha$ . The second model requires gain values corresponding to the main and side lobes,  $G_1$  and  $G_2$ , associated with a chosen directivity angle  $\alpha$  and the power loss parameter to back and side lobes  $k$ .

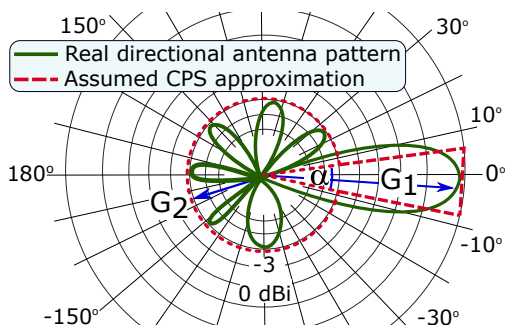
The power spectral density (psd)  $P_R$  at a distance  $r$  is

$$P_R = \frac{P_A}{S_A} = \frac{P_A}{2\pi r h}, \quad (22)$$

where  $\alpha$  is the antenna directivity,  $P_A$  is the emitted power, and  $S_A$  is the area of the wavefront surface. The latter is known to be  $h = r[1 - \cos(\alpha/2)]$ . By applying the free-space



(a) 2D cone antenna model



(b) 2D cone-plus-sphere model

Fig. 10. Illustration of the 2D approximate antenna models.

propagation model (FSPL), the power spectral density at the wavefront surface  $P_R$  is given by

$$P_R = \frac{P_A}{S_A} = P_A \frac{G}{4\pi r^2}, \quad (23)$$

leading to the following for the main lobe gain

$$G = \frac{2}{1 - \cos(\alpha/2)}. \quad (24)$$

Consider now the 2D cone-plus-sphere model. Let  $k_1$  and  $k_2$  denote the fractions of power split between the main lobe and back and side lobes, i.e.,  $k_1 + k_2 = 1$ . By applying the same logic as in the case of the cone model we may write

$$\begin{cases} P_{R,1} 2\pi r^2 [1 - \cos(\alpha/2)] = k_1 P_A \\ P_{R,2} 2\pi r^2 [1 + \cos(\alpha/2)] = k_2 P_A \\ k_1 + k_2 = 1 \end{cases}, \quad (25)$$

where, according to the FSPL, we have

$$\begin{cases} P_{R,1} = G_1 P_A / 4\pi r^2 \\ P_{R,2} = G_2 P_A / 4\pi r^2 \end{cases}. \quad (26)$$

Thus, there exists the following relationship

$$G_1 [1 - \cos(\alpha/2)] + G_2 [1 + \cos(\alpha/2)] = 2. \quad (27)$$

Using  $k = k_1/k_2$  we see that  $G_2 = kG_1$  and  $G_1, G_2$  are

$$\begin{cases} G_1 = 2[(1 - \cos(\alpha/2)) + k(1 + \cos(\alpha/2))]^{-1} \\ G_2 = kG_1 \end{cases}. \quad (28)$$

2) *3D Models*: One of the critical issues of the considered models is their 2D nature implying that they cannot be utilized for mmWave and, especially, THz systems featuring antennas forming radiation patterns in horizontal and vertical dimensions, simultaneously. Following [75], [74] we consider an antenna pattern approximated by a pyramidal zone, see Fig. 9. This model is fully defined by angles,  $\alpha_V$  and  $\alpha_H$ .

To obtain the gain  $G$  as a function of  $\alpha_V$  and  $\alpha_H$ , we first notice that the wavefront surface area is provided by the area of the spherical rectangle, see Fig. 9. Applying the law of cosines [135], we obtain  $\cos \chi$  as

$$\begin{aligned} \cos \chi &= \frac{\cos\left(\frac{\pi}{2} - \frac{L_H}{2}\right) - \cos\left(\frac{\pi}{2} - \frac{L_H}{2}\right) \cos(L_V)}{\sin\left(\frac{\pi}{2} - \frac{L_H}{2}\right) \sin(L_V)} = \\ &= \frac{\sin\left(\frac{L_H}{2}\right) (1 - \cos(L_V))}{\cos\left(\frac{L_H}{2}\right) \sin(L_V)} = \\ &= \tan\left(\frac{L_H}{2}\right) \tan\left(\frac{L_V}{2}\right). \end{aligned} \quad (29)$$

The quarter of the spherical excess is  $(\rho - \pi/2)$  leading to

$$\cos\left(\rho - \frac{\pi}{2}\right) = \tan\left(\frac{L_H}{2}\right) \tan\left(\frac{L_V}{2}\right), \quad (30)$$

where  $L_H$  and  $L_V$  are spherical geodesics corresponding  $\alpha_H$  and  $\alpha_V$ . Hence the sought area is

$$S_A = 4 \arcsin\left(\tan\left(\frac{\alpha_V}{2}\right) \tan\left(\frac{\alpha_H}{2}\right)\right). \quad (31)$$

Since the wavefront psd is provided as  $P_R = Ar^{-\zeta}$ , the gain of the main lobe is obtained as follows

$$G(\alpha_V, \alpha_H) = \frac{4\pi}{S_A} = \frac{\pi}{\arcsin\left(\tan\left(\frac{\alpha_V}{2}\right) \tan\left(\frac{\alpha_H}{2}\right)\right)}. \quad (32)$$

TABLE II  
ANTENNA HPBW AND ITS APPROXIMATION, REPRODUCED FROM [137]

Array	Value, direct calculation	Approximation
64x1	1.585	1.594
32x1	3.171	3.188
16x1	6.345	6.375
8x1	12.71	12.75

3) *Antenna Parameterization*: The introduced antenna arrays model requires directivity angles as the input,  $\alpha$  for 2D antenna models and  $\alpha_V$  and  $\alpha_H$  for 3D antenna models. To determine them, recall that HPBW of the antenna array is determined by the number of antenna elements in the considered plane. By utilizing the array maximum  $\theta_m$  and the 3-dB point,  $\theta_{3db}$ , the following relation holds for the HPBW of the linear array [136]

$$\alpha = 2|\theta_m - \theta_{3db}|, \quad (33)$$

where  $\theta_m$  is related to the phase excitation difference,  $\beta$  as

$$\theta_m = \arccos(-\beta/\pi), \quad (34)$$

leading to  $\theta_m = \pi/2$  for  $\beta = 0$ .

The upper and lower 3-dB points are given by [136]

$$\theta_{3db}^{\pm} = \arccos[-2.782/(N\pi)]. \quad (35)$$

Table II shows HPBWs and their approximation via empirical law  $102/N$  for linear arrays, where  $N$  specifies the number of array elements. We also note that instead of calculating the antenna gains for considered models analytically based on wavefront area one may utilize [136]

$$G = \frac{1}{\theta_{3db}^+ - \theta_{3db}^-} \int_{\theta_{3db}^-}^{\theta_{3db}^+} \frac{\sin(N\pi \cos(\theta)/2)}{\sin(\pi \cos(\theta)/2)} d\theta. \quad (36)$$

The antenna gains are summarized in Table III.

### G. Beamsearching Algorithms

The beam misalignment caused by micromobility and blockage affects the already strict time budget for beamtracking in mmWave and THz communications. Inherently requiring high gains at both BS and UE sides, these systems would require antenna arrays with tens (mmWave band) or even hundreds (THz band) of array elements to form "pencil-wide" beams [11]. This would lead to extremely large beamforming codebooks at both communications sides drastically increasing the beamsearching time. This time can be reduced by minimizing the arrays switching time. However, given the expected an order of magnitude increase in the number of antenna array elements, the arrays switching time has to be

TABLE III  
ANTENNA ARRAY GAINS, REPRODUCED FROM [137]

Array	Gain, linear	Gain, dB
64x1	57.51	17.59
32x1	28.76	14.58
16x1	14.38	11.57
8x1	7.20	8.57
4x1	3.61	5.57

decreased down to nanoseconds from the current state-of-the-art few microseconds that may not be feasible for modern arrays design options [138], [139].

The algorithmic beamtracking improvements are nowadays considered as the main option for efficient utilization of mmWave and THz resources. The approaches originally proposed for beamtracking design in mmWave systems, in addition to hierarchical iterative mechanisms putting one of the sides in omnidirectional regime similarly to IEEE 802.11ad/ay technologies [140], [141] and various algorithmic improvements [142], [143], may utilize: (i) external localization information provided by e.g., GPS or 5G/6G positioning services [144], [145], [146] or radar information [147], (ii) lower-band RATs for provisioning of direction towards BS/UE [148], [149], (iii) information available in the past when the connection has been up [150], [151], [152].

To abstract specifics of the beamsearching procedure, models for performance evaluation purposes need to specify two parameters as a function of beamsearching algorithm and antenna array: (i) beamsearching time and (ii) time instance when beamsearching is initiated. Consider exhaustive search as an example. Here, to establish a direction to the BS, both UE and BS need to attempt all feasible configurations leading to the beamsearching time of  $T_S = N_U N_A \delta$ , where  $N_U$  and  $N_A$  are the number of UE and BS configurations and  $\delta$  is the array switching time. For hierarchical search, UE and BS perform beamsearching by switching the other side to omnidirectional mode. Here, the beamsearching time is  $T_S = (N_U + N_A)\delta$ . By analogy, the beamsearching time of any algorithm can be defined as a function (possibly probabilistic) of  $N_U$ ,  $N_A$  and  $\delta$ . As one may deduce, the array switching time,  $\delta$ , is a crucial parameter for future mmWave and THz systems. In general, it heavily depends on array implementation and may vary on the timescale from microseconds to milliseconds. As an example, IEEE 802.11ad recommends utilizing arrays with  $\delta = 1$  ms leading to 4 ms and 0.41 ms of beamsearching time for exhaustive and hierarchical search, respectively, and 64 and 4 antenna elements at BS and UE sides.

Addressing the time, when beamsearching is initiated we distinguish between two system design options, cellular and WLANs [19]. In the former case, beamsearching is performed periodically with interval  $T_P$ . Note that the frame duration in mmWave NR and THz systems (1 ms for mmWave NR [153] and might get smaller for THz radio interface) is smaller than the time to the outage, caused by the micromobility reported in [19]. Thus, in this case, one may assume that only blockage leads to outage situations. According to WLAN design [140], beamsearching is performed once the connection is lost. Thus, not only blockage but micromobility may cause an outage.

### H. Metrics of Interest

Performance of previous generations of cellular systems, e.g., LTE, have been evaluated assuming elastic traffic patterns inherently adaptive to the network state and thus mainly utilized the elements of stochastic geometry [31], [32]. In such systems performance metrics of interest are related to principal connectivity measures of UEs, i.e., outage and coverage probabilities, spectral efficiency, Shannon channel capacity, and

fairness of resource allocations, etc., as a function of UE and BS densities. Evaluating performance of non-elastic applications at the air interface with high and guaranteed bitrates over mmWave and THz air interfaces prone to outage events requires not only to take into account radio part specifics but the traffic service dynamics at BSs by joining the tools of stochastic geometry and queuing theory.

Performance evaluation frameworks for mmWave and THz systems need to address both user- and system-centric KPIs. For user-centric KPI one may consider: (i) the new session drop probability and (ii) the ongoing session drop probability. The former is defined as the probability that a new session arriving session to BS is lost due to the lack of resources needed to serve it. The ongoing session drop probability is interpreted as the probability that a session already accepted for service is lost during the ongoing service. These metrics describe the so-called session continuity of applications characterizing how reliable the provided service is and can be used to benchmark the advanced service mechanisms at BSs [84], [54], [57], [154]. Finally, the system-centric KPIs in these systems are mainly related to the efficiency of resource utilization at BSs.

#### IV. PERFORMANCE EVALUATION MODELS

In this section, we introduce the performance evaluation models suitable for performance assessment of traffic service performance at mmWave/THz BSs. We start by describing the overall structure of the framework defining the type of models, requirements and interfaces between them. Then, we treat in detail the models suitable for baseline, multiconnectivity, resource reservation functionalities as well as priority-based service with traffic differentiation capabilities.

##### A. Methodology at the Glance

We will consider a performance evaluation framework capable of quantifying the user- and system-centric KPI defined in Section III. The overall framework is divided into two complementary parts: (i) a queuing part specified in this section and (ii) a radio abstraction (parametrization) part introduced in Section V. The latter captures the specifics of propagation properties of mmWave/THz bands as well as additional phenomena such as micromobility and blockage. The queuing part characterizes the resource allocation dynamics at the BS and accepts the pmf of the amount of requested resources,  $\{p_j\}_{j \geq 0}$ , and the temporal intensity of the UE stage changes between outage and non-outage conditions,  $\alpha$ , as the input. The former parameter is responsible for abstracting the random UE locations with respect to BSs in the deployment of interest as well as antenna and propagation specifics. The latter parameter is responsible for capturing outage prone nature of considered RATs caused by blockage and micromobility dynamics. Thus, these two parameters characterize the type of deployment providing the interface between two parts of the framework. Supplementing these two with the conventional session arrival and service characteristics that are not directly related to the radio part, the intensity of session arrivals,

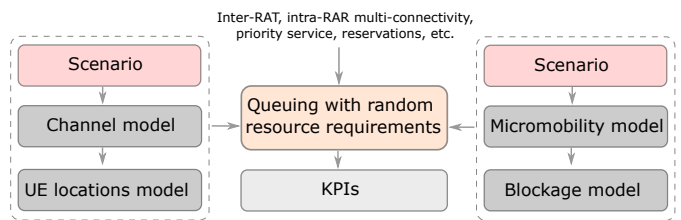


Fig. 11. Illustration of the general structure of the framework.

session services times, and required rate of sessions, one fully specifies the framework.

The overall structure of the proposed framework is illustrated in Fig. 11. By design, it allows for reuse of the core parts for investigating alternative mmWave/THz deployments by selecting appropriate models specified in the previous section. Here, the radio abstraction part estimates the intermediate “interface” parameters as a function of the considered deployment scenario, selected models as well as the system and environmental characteristics. As a result, the framework delivers KPIs of interest for selected advanced resource allocation policies at the BS, i.e., the resource reservation fraction, the number of simultaneously supported links, priorities, etc.

The queuing framework is characterized by a hierarchical structure. The baseline considered below first introduces the model with a single traffic type, no priorities and no session continuity mechanisms. Then, we proceed gradually extending the baseline to more sophisticated scenarios in incremental order of complexity, first, to resource reservation, then to multiconnectivity, further – to priorities. Note that additional models can be built on top of these, e.g., by uniting multiconnectivity and priorities and defining additional rules to utilizing the former, one could formalize a model of a network segment with multiconnectivity capabilities servicing two or more traffic types.

The framework is based on resource queuing systems (RQS). The main difference between RQS and conventional queuing systems is that sessions require not only a server but also some random volume of a finite resource. This difference makes it possible to take into account the heterogeneity of the session resource requirements at mmWave/THz BSs arising from the random locations of UEs and, as a consequence, the random spectral efficiency of the wireless channel associated with the data sessions.

Note that this part does not pretend to be a complete review of the RQS theory. We present only the main results that are most often used in the analysis of mmWave/THz networks. We invite the interested reader to refer to the review of the RQS in two parts [155], [156], which describes in detail the state-of-the-art of the RQS theory.

##### B. Baseline Resource Queuing Systems

First, we consider a baseline resource model, see Fig. 12, that is, a multiserver queuing system with  $N \leq \infty$  servers and a finite volume of resources,  $R$ . Assume that the arriving flow is Poisson with parameter  $\lambda$ , and service times of sessions are independent of each other, independent of the arrival process, and are exponentially distributed with parameter  $\mu$ .

Each session requires one server and a random volume of the resources. Here, the amount of servers may represent the maximum number of active connections, if there is such a limit, while resources abstract time-frequency resources at the air interface and can be expressed in terms of resource blocks (RB). In what follows, we will assume that the distribution of resource requirements by a session is discrete and is described by the pmf  $\{p_j\}_{j \geq 0}$ , where  $p_j$  is the probability that the session requires  $j$  resource units. An arriving session is lost if the amount of resource required for it exceeds the amount of unoccupied resources. At the end of the service, the session leaves the system and the total amount of occupied resources is decreased by the amount of resources allocated to the session. The schematic illustration of the considered system is shown in Fig. 12. Note that this model captures only the randomness of session resource requirements caused by UE locations, propagation model, utilized antenna arrays and session rate.

The system behavior is described by a random process  $X_1(t) = \{\xi(t), \gamma(t)\}$ , where  $\xi(t)$  is the number of sessions in the system at the time  $t$ , and  $\gamma(t) = (\gamma_1(t), \dots, \gamma_{\xi(t)}(t))$  is the vector that represents the number of resources allocated to each session. Let us introduce the notation for the stationary distribution of the process  $X_1(t)$

$$Q_k(r_1, \dots, r_k) = \lim_{t \rightarrow \infty} P \{ \xi(t) = k, \gamma_1(t) = r_1, \dots, \gamma_k(t) = r_k \}. \quad (37)$$

In [157] it was shown that stationary probabilities (37) can be obtained as follows

$$Q_k(r_1, \dots, r_k) = Q_0 \frac{\rho^k}{k!} \prod_{i=1}^k p_{r_i}, \quad 1 \leq k \leq N, \sum_{i=1}^k r_i \leq R, \\ Q_0 = \left( 1 + \sum_{k=1}^N \sum_{r_1 + \dots + r_k \leq R} \frac{\rho^k}{k!} \prod_{i=1}^k p_{r_i} \right)^{-1}, \quad (38)$$

where  $\rho = \lambda/\mu$  is the offered load.

Note that the state space of the process  $X_1(t)$  grows very quickly with the increase in  $N$  and  $R$ , which leads to significant difficulties in calculating the stationary probabilities and the performance measures of the system, despite availability of analytical expressions in (38). Moreover, the process  $X_1(t)$  includes a lot of redundant information, which is unnecessary in most cases. By applying the state aggregation technique [158], [159], to analyze the performance indicators of the system, it is sufficient to track only the number of sessions in the system and the total amount of the resource occupied by all the sessions. The stationary probabilities for the aggregated states are provided by

$$P_k(r) = \lim_{t \rightarrow \infty} P \left\{ \xi(t) = k, \sum_{i=1}^k \gamma_i(t) = r \right\}. \quad (39)$$

By summing up the probabilities in (38), we obtain

$$P_k(r) = P_0 \frac{\rho^k}{k!} p_r^{(k)}, \quad 1 \leq k \leq N, r \leq R, \\ P_0 = \left( 1 + \sum_{k=1}^N \sum_{r=0}^R \frac{\rho^k}{k!} p_r^{(k)} \right)^{-1}, \quad (40)$$

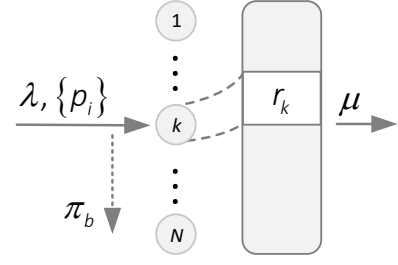


Fig. 12. Illustration of the baseline resource queuing system.

where  $\{p_r^{(k)}\}_{r \geq 0}$  is a  $k$ -fold convolution of distribution  $\{p_j\}_{j \geq 0}$ . Note that  $p_r^{(k)}$  can be interpreted as the probability that  $k$  sessions totally occupy  $r$  resources. In practice, discrete convolutions are calculated using the recurrence relation

$$p_r^{(k)} = \sum_{i=0}^r p_i p_{r-i}^{(k-1)}, \quad k \geq 2, \quad (41)$$

where  $p_r^{(1)} = p_r$ ,  $r \geq 0$ .

Using the probabilities of the aggregated states  $P_k(r)$ , we can obtain expressions for the main characteristics of the model, namely, the new session drop probability  $\pi_b$  and the average number of occupied resources  $\bar{R}$  as follows

$$\pi_b = 1 - P_0 \sum_{k=0}^{N-1} \frac{\rho^k}{k!} \sum_{r=0}^R p_r^{(k+1)}, \quad (42)$$

$$\bar{R} = P_0 \sum_{k=1}^N \frac{\rho^k}{k!} \sum_{r=1}^R r p_r^{(k)}. \quad (43)$$

*1) Simplified System:* Consider a simplified process  $X_2(t) = \{\xi(t), \delta(t)\}$ , where, differently from  $X_1(t)$  considered above, the second component  $\delta(t)$  denotes the total number of resources occupied by all the sessions. This simplification leads, on the one hand, to the decrease in the dimension of the state space, and, on the other hand, to the loss of important information about the queuing process. As a result, it is impossible to say exactly how many resources are released by a session upon its departure. In this case, one may utilize the following Bayesian approach. Assume that the system is in the state  $(k, r)$  at the moment just before the session departure from the system. The probability that a session will release  $j$  resources can be determined by the Bayes formula as  $p_j p_{r-j}^{(k-1)} / p_r^{(k)}$ . Then, the system of equilibrium equations for stationary probabilities  $q_k(r)$  of the process  $X_2(t)$  can be written in the following form

$$\lambda q_0 \sum_{r=0}^R p_r = \mu \sum_{r=0}^R q_1(r), \\ q_k(r) \left( \lambda \sum_{r=0}^{R-r} p_r + k\mu \right) = \lambda \sum_{j=0}^r q_{k-1}(j) p_{r-j} + (k+1) \times \\ \times \mu \sum_{j=0}^{R-r} q_{k+1}(r+j) \frac{p_j p_r^{(k)}}{p_{r+j}^{(k+1)}}, \quad 1 \leq k \leq N-1, 0 \leq r \leq R, \\ N\mu q_N(r) = \lambda \sum_{j=0}^r q_{N-1}(j) p_{r-j}, \quad 0 \leq r \leq R. \quad (44)$$

As shown in [157], by substituting  $P_k(r)$  from (39) into the system (44), one can prove that (40) is its solution. Thus, the stationary probabilities of the simplified process  $X_2(t)$  coincide with the probabilities of the aggregated states  $P_k(r)$  of the initial process  $X_1(t)$ . As we will see in the following sections, the established fact is of critical importance for the analysis of more complex systems involving additional rules and service mechanisms at BSs. Generally, in more complex systems, it is not possible to obtain analytical expressions for stationary probabilities, which means that to analyze those systems one has to resort to a numerical solution of the system of equilibrium equations. However, in most practical cases it is not feasible due to the large state space of the process. Therefore, the proposed simplification makes it possible to numerically calculate performance measures of the considered class of systems in a reasonable time.

2) *Multiple Arriving Flows*: Consider now a resource queuing system with multiple arriving flows of sessions. Particularly, differently from the systems considered above, we assume  $L$  arriving mutually independent Poisson flows of sessions with intensities  $\lambda_l$ ,  $l = 1, 2, \dots, L$ . Sessions of the  $l$ -th type are served with rates  $\mu_l$ , and their distribution of resource requirements is given by  $\{p_{l,r}\}_{r \geq 0}$ . The stationary probabilities  $Q_{k_1, \dots, k_L}(r_1, \dots, r_L)$  that there are  $k_l$  sessions of type  $l$  occupying totally  $r_l$  resources,  $l = 1, 2, \dots, L$ , are then provided by

$$Q_{k_1, \dots, k_L}(r_1, \dots, r_L) = Q_0 \prod_{i=1}^L \frac{\rho_i^{k_i}}{k_i!} \prod_{i=1}^L p_{r_i}^{(k_i)}, \sum_{l=1}^L k_l \leq N, \sum_{l=1}^L r_l \leq R, \quad (45)$$

$$Q_0 = \left( 1 + \sum_{1 \leq k_1 + \dots + k_L \leq N} \sum_{0 \leq r_1 + \dots + r_L \leq R} Q_{k_1, \dots, k_L}(r_1, \dots, r_L) \right)^{-1}.$$

where  $\rho_l = \frac{\lambda_l}{\mu_l}$ ,  $l = 1, 2, \dots, L$ .

Note that (45) are also not overly useful for numerical calculations. However, in [160], it was shown that a resource queuing system with  $L$  flows of sessions is equivalent to the resource queuing system with one aggregated flow having a weighted average distribution of resource requirements. In other words, the stationary probabilities  $Q_k(r)$  that there are  $k$  sessions of all types in the system that totally occupy  $r$  resources, are determined by

$$Q_k(r) = Q_0 \frac{\rho^k}{k!} \bar{p}_r^{(k)}, 1 \leq k \leq N, r \leq R$$

$$Q_0 = \left( 1 + \sum_{k=1}^N \sum_{r=0}^R Q_k(r) \right)^{-1}, \quad (46)$$

where  $\rho = \rho_1 + \dots + \rho_L$ , and  $\bar{p}_r$  are given by

$$\bar{p}_r = \sum_{l=1}^L \frac{\rho_l}{\rho} p_{l,r}. \quad (47)$$

The mean amount of occupied resources can be found similarly to (42), and the session drop probability of a  $l$ -type

session takes the form of

$$\pi_{b,l} = 1 - \sum_{k=0}^{N-1} \sum_{r=0}^R Q_k(r) p_{l,R-r}. \quad (48)$$

3) *Numerical Algorithm*: The direct calculation of performance measures associated with resource queuing systems is complicated. The main reason is the need for evaluating multiple convolutions of the resource requirements distribution as discussed above. However, the authors in [161], developed a recursive algorithm for calculating the normalization constant  $Q_0$ , which allows for efficient numerical analysis.

The algorithm proceeds as follows. First, denote

$$G(n, r) = \sum_{k=0}^n \frac{\rho^k}{k!} \sum_{j=0}^r p_j^{(k)}. \quad (49)$$

Utilizing this notation, the normalization constant in (46), interpreted as the probability that the system is empty, can be written as  $Q_0 = G(N, R)^{-1}$ . The function  $G(n, r)$  can be calculated using the following recursion

$$G(n, r) = G(n-1, r) + \frac{\rho}{n} \sum_{j=0}^r p_j (G(n-1, r-j) - G(n-2, r-j)), \quad (50)$$

with initial conditions

$$G(0, r) = 1, \quad G(1, r) = 1 + \sum_{j=0}^r p_j, \quad r \geq 0. \quad (51)$$

Using  $G(n, r)$ , any performance measure of the system can be calculated. For example, the session drop probability  $\pi_b$  and the average amount of occupied resources  $\bar{R}$  take the form

$$\pi_b = 1 - \frac{1}{G(N, R)} \sum_{j=0}^R p_j G(N-1, R-j),$$

$$\bar{R} = R - \frac{1}{G(N, R)} \sum_{j=1}^R G(N, R-j). \quad (52)$$

### C. Resource Queuing System with Service Interruptions

Consider now the extension of the system to the case of external flow of events that may potentially change the characteristics of the service process of sessions, currently served at the BS. In mmWave and THz systems these events can be utilized to capture impairments caused by the blockage process of LoS path, leading to either change in the resource requirements to maintain the target session rate [57], [54] or to outage events completely interrupting the session service process [154]. In addition, these events can also model outage events caused by micromobility [19], [20]. Due to a wide scope of the application area of these systems, in what follows, the external events are referred to as ‘‘signals’’.

Unlike the model considered in Section IV-B, we assume that each session is associated with a Poisson flow of signals with intensity  $\alpha$ . For certainty, in further exposition we consider LoS blockage process associated with UEs, where the blockage does not lead to outage conditions, i.e., in case



$$\begin{aligned}
\mathbf{D}_n(I(n, i), (n, j)) &= \begin{cases} - \left( \lambda \sum_{j=0}^{R-i} p_j + n\mu + n\alpha \left( 1 - \sum_{m=0}^i \theta_m(n, i) p_m \right) \right), & i = j, \\ n\alpha \sum_{m=0}^i \theta_m(n, i) p_{j-i+m}, & i < j, \\ n\alpha \sum_{m=i-j}^i \theta_m(n, i) p_{j-i+m}, & i > j, \end{cases} & (n, i), (n, j) \in \Psi_n, \quad 1 \leq n \leq N-1, \\
\mathbf{D}_N(I(N, i), (N, j)) &= \begin{cases} - \left( N\mu + N\alpha \left( 1 - \sum_{m=0}^i \theta_m(N, i) p_m \right) \right), & i = j, \\ N\alpha \sum_{m=0}^i \theta_m(N, i) p_{j-i+m}, & i < j, \\ N\alpha \sum_{m=i-j}^i \theta_m(N, i) p_{j-i+m}, & i > j, \end{cases} & (N, i), (N, j) \in \Psi_N. \quad (53)
\end{aligned}$$

of blockage the connection may still be maintained but more resources are required to provide the target session rate. In this case, upon signal arrival, the resources allocated for a session are all released and the session tries to occupy a new volume of resources according to the same or different probability distributions. In what follows, for certainty, we assume that the distribution remains intact. Note that this could be a pmf of session resource requirements obtained for blocked and non-blocked states and then weighted with blockage probability as discussed in Section V.

For analysis of this system, one may utilize the simplified method considered in Section IV-B1 that implies tracking only the total amount of the occupied resources. Accordingly, the behavior of the system is described by the stochastic process  $X(t) = \{\xi(t), \delta(t)\}$ , where the first component denotes the number of sessions in the system at time  $t$ , and the second represents the total amount of resources occupied by all the sessions. The state space of the system is given by

$$\Psi = \bigcup_{k=0}^N \Psi_k, \quad \Psi_k = \left\{ (k, r) : 0 \leq r \leq R, p_r^{(k)} > 0 \right\}, \quad (54)$$

where the states in the subsets  $\Psi_k$  are ordered according to the ascending of the number of resources. Let  $I(k, r)$  denote the sequential number of the state  $(k, r)$  in the set  $\Psi_k$ .

1) *Stationary Distribution*: First, we introduce an supplementary variable facilitating our exposition in what follows. Let  $\theta_i(k, r)$  be the probability that a session occupies  $i$  resources, provided that  $k$  sessions totally occupy  $r$  resources. Then, according to Bayes' law we have

$$\theta_i(k, r) = \frac{p_i p_{r-i}^{(k-1)}}{p_r^{(k)}}. \quad (55)$$

To construct the infinitesimal generator of the process  $X(t)$ , consider possible transitions between the states of the system in more detail. Let the system be in the state  $(k, r)$  at some time  $t$ . With probability  $p_j$ , an arriving session occupies  $j$  resources,  $j \leq R - r$ , and the system goes to the state  $(k + 1, r + j)$ . On the departure of a session, it releases  $i$  resources with probability  $\theta_i(k, r)$ . In this case, the system

state changes to the state  $(k - 1, r - i)$ . Upon signal arrival, a session releases  $i$  resources with probability  $\theta_i(k, r)$  and requests  $j$  resources with probability  $p_j$ . If  $j \leq i$ , then the session continues its service the system. If  $j < i$ , the system state changes to  $(k, r - i + j)$  with probability  $\theta_i(k, r) p_j$  while in the case of  $j = i$  the state of the system does not change. Finally, if the new volume of resources requested by a session exceeds its previous volume ( $j > i$ ), then the session remains in the system only when  $j \leq R - r + i$ . Otherwise, the session is lost (dropped) and the system goes to the state  $(k - 1, r - i)$ .

The infinitesimal generator of the process  $X(t)$  is a block tridiagonal matrix with diagonal blocks  $\mathbf{D}_0, \mathbf{D}_1, \dots, \mathbf{D}_N$ , superdiagonal blocks  $\mathbf{\Lambda}_1, \dots, \mathbf{\Lambda}_N$  and subdiagonal blocks  $\mathbf{M}_0, \dots, \mathbf{M}_{N-1}$ , provided by

$$\begin{aligned}
\mathbf{D}_0 &= -\lambda \sum_{j=0}^R p_j, \\
\mathbf{\Lambda}_1 &= (\lambda p_0, \dots, \lambda p_R), \\
\mathbf{M}_0 &= (\mu, \dots, \mu)^T. \quad (56)
\end{aligned}$$

Omitting zero elements from the block  $\mathbf{\Lambda}_1$ , the number of columns in  $\mathbf{\Lambda}_1$ , as well as the number of rows in the block  $\mathbf{M}_0$ , are equal to the number of states in the subset  $\Psi_1$ . The blocks  $\mathbf{D}_n(I(n, i), (n, j))$  and  $\mathbf{D}_N(I(N, i), (N, j))$  are provided in (53). The blocks  $\mathbf{\Lambda}_n(I(n-1, i), (n, j))$  are provided by

$$\mathbf{\Lambda}_n(I(n-1, i), (n, j)) = \begin{cases} \lambda p_{j-i}, & i \leq j \leq R, \\ 0, & j < i, \end{cases} \quad (58)$$

where  $(n-1, i) \in \Psi_{n-1}$ ,  $(n, j) \in \Psi_n$ ,  $2 \leq n \leq N$ .

Finally, the blocks  $\mathbf{M}_n(I(n+1, i), (n, j))$  are specified as

$$\begin{aligned}
\mathbf{M}_n(I(n+1, i), (n, j)) &= \\
&= \begin{cases} (n+1)\mu\theta_{i-j}(n+1, i), & j \leq i \leq R, \\ 0, & j > i, \end{cases} \quad (59)
\end{aligned}$$

where  $(n+1, i) \in \Psi_{n+1}$ ,  $(n, j) \in \Psi_n$ ,  $1 \leq n \leq N-1$ .

The stationary probabilities  $Q_k(r)$  of the process  $X(t)$  are the unique solution of the system of equilibrium equations with the normalization condition, that can be written as

$$\mathbf{Q}\mathbf{A} = \mathbf{0}, \quad \mathbf{Q}\mathbf{1} = 1, \quad (60)$$

$$\begin{aligned}
\text{(i)} \quad & \lambda Q_0 \sum_{j=0}^{R_0} p_j = \mu \sum_{j:(1,j) \in \Psi_1} Q_1(j) + \alpha \sum_{j:(1,j) \in \Psi_1} Q_1(j) \left( 1 - \sum_{s=0}^R p_s \right), \\
\text{(ii)} \quad & \left( \theta(R_0 - j) \lambda \sum_{j=0}^{R_0-r} p_j + k\mu + k\alpha \right) Q_k(r) = \theta(R_0 - j) \lambda \sum_{j \geq 0: (k-1, r-j) \in \Psi_{k-1}} Q_{k-1}(r-j) p_j + (k+1)\mu \times \\
& \times \sum_{j \geq 0: (k+1, r+j) \in \Psi_{k+1}} Q_{k+1}(r+j) \theta_j(k+1, j+r) + (k+1)\alpha \left( 1 - \sum_{s=0}^{R-r} p_s \right) \sum_{j \geq 0: (k+1, r+j) \in \Psi_{k+1}} Q_{k+1}(r+j) \theta_j(k+1, j+r) + \\
& + k\alpha \sum_{j \geq 0: (k,j) \in \Psi_k} Q_k(j) \sum_{i=0}^{\min(j,r)} \theta_{j-i}(k+1, j+r) p_{r-i}, \quad 1 \leq n \leq N-1, \quad 0 \leq r \leq R, \\
\text{(iii)} \quad & N(\mu + \alpha) Q_N(r) = \theta(R_0 - j) \lambda \sum_{j \geq 0: (N-1, j) \in \Psi_{N-1}} Q_{N-1}(r-j) p_j + N\alpha \sum_{j \geq 0: (N, j) \in \Psi_N} Q_N(j) \sum_{i=0}^{\min(j,r)} \theta_{j-i}(N, j) p_{r-i}, \quad 1 \leq r \leq R.
\end{aligned} \tag{57}$$

where  $\mathbf{Q}$  is the row vector of stationary probabilities,  $\mathbf{1}$  is a column vector of ones of appropriate size. The system (60) can be solved by any numerical method, including those using the special block structure of the described infinitesimal generator.

2) *Performance Metrics*: In this subsection, we will proceed to the analysis of system's performance indicators including the drop probability of a session upon arrival,  $\pi_b$ , and the average amount of occupied resources,  $\bar{R}$ . These metrics can be directly calculated using stationary probabilities as

$$\begin{aligned}
\pi_b &= 1 - \sum_{k=0}^{N-1} \sum_{r=0}^R Q_k(r) \sum_{j=0}^{R-r} p_r, \\
\bar{R} &= \sum_{k=0}^N \sum_{r=0}^R r Q_k(r).
\end{aligned} \tag{61}$$

In the considered system, we are also interested in the probability  $\pi_t$  that a session initially accepted for service is eventually lost due to the signal arrival. In our interpretation, this implies that upon blockage, the amount of resources at BS is insufficient to maintain the target bitrate of the session. To derive this metric, we first calculate the intensity of sessions that are eventually dropped,  $\nu$ , as

$$\nu = \alpha \bar{N} \sum_{k=1}^N \sum_{r=0}^R Q_k(r) \sum_{j=0}^r \theta_j(k, r) \left( 1 - \sum_{i=0}^{R-r+j} p_i \right), \tag{62}$$

where  $\bar{N}$  is the mean number of sessions in the system

$$\bar{N} = \sum_{k=1}^N \sum_{r=0}^R k Q_k(r). \tag{63}$$

Then, the sought probability  $\pi_t$  can be defined as the limit of the ratio of the number of accepted sessions that have been eventually dropped to the total number of accepted sessions during the time interval of duration  $T$ . Accordingly, we have

$$\pi_t = \lim_{T \rightarrow \infty} \frac{\nu T}{\lambda(1 - \pi_b)T} = \frac{\nu}{\lambda(1 - \pi_b)}. \tag{64}$$

We specifically note that the probability that a session initially accepted to the system is eventually dropped is known to drastically affect quality of user experience (QoE) of a service [162], [163], [164], [165]. As these events may often happen in mmWave and THz communications, recently, a number of approaches for improving it have been proposed. Most of these mechanisms can be modeled by utilizing the resource queuing systems framework described above. In what follows, we consider some of these mechanisms as examples.

#### D. Resource Reservation

Reserving resources for sessions that sharply increase their resource requirements due to blockage of a LoS path, is one of the mechanisms to improve session continuity in mmWave and THz systems [57], [53], especially, in early rollouts of these systems, where BS will be sparsely deployed. In this case, only part of the BS resources is available for the new arriving sessions, and the rest is reserved to support the sessions already accepted for service.

1) *Model Description*: Consider a resource queuing system with  $N$  servers and a finite amount of resources  $R$ , only part of which  $R_0 = (1 - \gamma)R$ ,  $0 < \gamma < 1$ , is available for new arriving sessions. Here  $\gamma$  is the reservation coefficient and is interpreted as a fraction of reserved resources. The behavior of the system is described by a stochastic process  $X(t) = \{\xi(t), \delta(t)\}$ , where  $\xi(t)$  is the number of sessions in the system, and  $\delta(t)$  is the total the amount of the occupied resource. The state space of the system is described by (54).

Unlike the system considered in Section IV-C, when a session arrives to the system, it can occupy only a part of the resources,  $R_0 < R$ . In other words, let the system be in the state  $(k, r)$  and assume that an arriving session requires  $j$  resources, then: (i) if  $r > R_0$ , any new arriving session is dropped, (ii) if  $r \leq R_0$  and  $j > R_0 - r$ , then an arriving session is dropped, and (iii) if  $r \leq R_0$  and  $j \leq R_0 - r$ , an arriving session is accepted into the system. Once the session

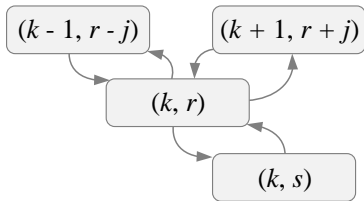


Fig. 13. Transitions for the central state of the model.

is accepted for service, the whole amount of resources,  $R$ , becomes available for it. When a signal arrives for a session when the system is in the state  $(k, r)$ , the session releases  $i$  resources and tries to occupy  $j$  resources. In this case, it is dropped only when  $j > R - r + i$ . Otherwise, the system operates similarly to the system described in Section IV-C. The typical subset of states and associated transitions for this system are illustrated in Fig. 13.

2) *Equilibrium Equations*: By utilizing

$$\theta(R_0 - j) = \begin{cases} 0, & j > R_0, \\ 1, & j \leq R_0, \end{cases} \quad (65)$$

the system of equilibrium equations can be written as in (57).

Using the system (57), together with the normalization condition provided in (65), one may calculate the stationary state probabilities of the system. Here, the infinitesimal generator of the process  $X(t) = \{\xi(t), \delta(t)\}$  is obtained similarly to Section IV-C based on the system of equations (57).

3) *Performance Metrics*: Consider the performance metrics of the system. Since the system with resource reservation differs from the system from Section IV-C only in the connection admission control (CAC) functionality, all the expressions for performance metrics except for the new session drop probability remain the same. The abovementioned unknown metric,  $\pi_b$ , is provided by

$$\pi_b = 1 - \sum_{k=0}^{N-1} \sum_{r=0}^{R_0} Q_k(r) \sum_{j=0}^{R_0-r} p_r, \quad (66)$$

4) *Illustrative Example*: An example of application of the abovementioned framework to the case of mmWave BS utilizing the resource reservation strategy for sessions already accepted to the system is considered in [57]. Consider a single cell system with session arrivals governed by the Poisson process whose geometric locations are uniformly distributed in the BS service area. Since resource reservation may only show gains when blockage does not lead to outage the cell service area is computed accordingly. In Fig. 14 we show typical new and ongoing session drop probabilities as a function of the amount of resources reserved for sessions accepted for service, required session rate of 10 Mbps and different blockers intensity in the environment,  $\lambda_B$  bl/m<sup>2</sup>. As one may observe, there is a clear trade-off between two considered types of session drop probabilities. Unfortunately, the new session drop probability increases at slightly faster rate as compared to the decrease in the ongoing session drop probability. Nevertheless, by utilizing this simple strategy a network operator may control the balance between these two

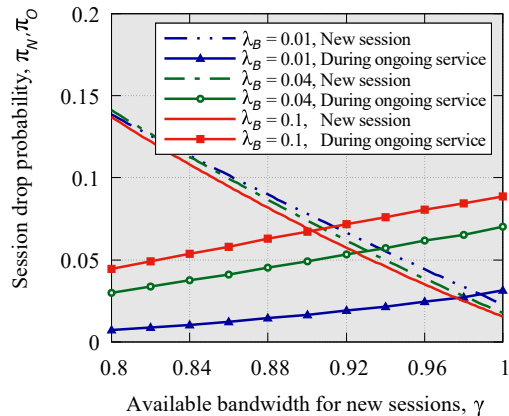


Fig. 14. New and ongoing session drop probabilities.

probabilities in early 5G mmWave systems rollouts when NR BSs are installed in hotspot areas with high traffic demands.

### E. Multiconnectivity and Resource Reservation

Another method for improving session continuity in mmWave and THz systems is a standardized by 3GPP multiconnectivity operation [50]. According to it, UE may maintain more than a single link to nearby BSs. UE may utilize all the links simultaneously via division duplex (TDD) mode or use one link for data transmission while keeping the rest as a backup options in the case the currently active link experiences outage conditions due to blockage and/or micromobility. These connectivity strategies and associated resource allocation policies fall within the class of resource queuing networks – an extension of resource queuing systems considered in the previous sections. Below, we describe the solution method for the case, where both multiconnectivity and resource reservation are simultaneously utilized.

1) *Model Description*: Consider a queuing network consisting of  $K$  BSs. The  $k$ -th BS has  $N_k$  servers and  $R_{k,1}$  resources. The  $k$ -th BS receives a Poisson flow of sessions with intensity  $\lambda_k$ ,  $k = 1, 2, \dots, K$ , and  $\lambda = \sum_{k=1}^K \lambda_k$ . Each session arriving to the  $k$ -th BS is characterized by a random resource requirements with pmf  $\{p_{0,r}\}_{r>0}$ . For new arriving sessions, only a part of the resources is available,  $R_{k,0} = R_{k,1}(1 - \gamma)$ ,  $0 < \gamma < 1$ . Similarly to the previous section, if an arriving session finds that there are not enough

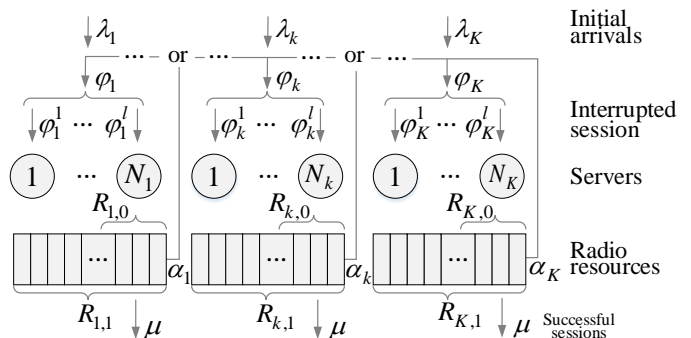


Fig. 15. Illustration of the resource queuing network.

resources in the system for its service, then this session is dropped. Service times are assumed to be exponentially distributed with the parameter  $\mu$ . Further, each session which is currently in service at the  $k$ -th BS is associated with a Poisson flow of signals with the intensity of  $\alpha_k$ ,  $k = 1, 2, \dots, K$ , that represents channel state transitions between outage and connectivity states that might be caused by either blockage or micromobility or both. Upon a signal arrival, the session releases the occupied resources and generates a new value of resource requirements according to pmf  $\{p_{1,r}\}_{r>0}$ . If these resources are not available at the current BS, session is routed to BS  $k$  with probability  $1/(K-1)$ . A rerouted sessions are called “secondary” sessions. We also introduce the “level” a secondary session as the number of reroutes a session experienced. Secondary sessions form an additional Poisson arriving flow to each BS with intensities  $\varphi_k$ ,  $k = 1, 2, \dots, K$ . All available resources at BSs are available for secondary sessions. If there is insufficient amount of resources available, the session is dropped. Due to the memoryless property of the exponential distribution, the residual service time of a secondary session also follows an exponential distribution with the same parameter  $\mu$ . Illustration of the considered model is sketched in Fig. 15.

To analyze the described model, we rely upon the network decomposition method, which is commonly utilized in the analysis of complex queuing networks [166], [167], [168]. As usual, the key assumption here is that the service process of sessions at each BS does not depend on the service processes at other BSs in the network. Based on the decomposition approach, we develop a recurrent algorithm for the evaluation of the performance metrics as shown in Fig. 16 and discussed below. First, the system parameters are initialized assuming the arrival intensity of the secondary sessions to be zero,  $\varphi_k = 0$ ,  $k = 1, 2, \dots, K$ . Then, the stationary probabilities of each BS are calculated, from which the network-wide measures are obtained. Further, the arrival intensities of the secondary sessions are recalculated by taking into account the next level of session rerouting. These new values of the arrival intensities  $\varphi_k = 0$ ,  $k = 1, 2, \dots, K$  are used at the next iteration of the algorithm. The algorithm stops as the difference between the

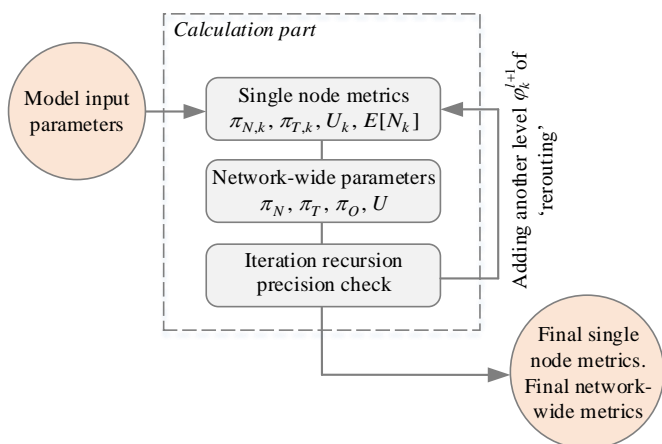


Fig. 16. Iterative algorithm for calculating performance metrics.

network characteristics at the consequent iterations becomes less than a certain specified level of accuracy.

2) *Single BS Performance*: Consider BS with two Poisson flows of sessions: the flows of primary and secondary sessions with rates  $\lambda_k$  and  $\varphi_k$ , respectively. By utilizing the memoryless property of exponential distribution we observe that the sojourn time of the session at the BS is also exponential with the parameter  $\mu + \alpha_k$ ,  $i = 1, 2, \dots, K$ . Here, we again apply the simplified approach, where only the total amount of the occupied resources is tracked at BS. Then, by taking into account the number of primary and secondary sessions, the behavior of the system is described by a three-dimensional process  $X(t) = \{\xi_1(t), \xi_2(t), \delta(t)\}$ , where  $\xi_1(t)$  is the number of primary sessions in the system at time  $t$ ,  $\xi_2(t)$  is the number of secondary sessions at time  $t$ , and  $\delta(t)$  is the total amount of the resource occupied by all the sessions. The state space of the process is thus given by

$$\Psi = \bigcup_{0 \leq n_1 + n_2 \leq N} \Psi_{n_1, n_2},$$

$$\Psi_{n_1, n_2} = \left\{ (n_1, n_2, r) : 0 \leq r \leq R_1, \sum_{i=0}^{\min(r, R_0)} p_{0,i}^{(n_1)} p_{1,r-i}^{(n_2)} > 0 \right\}, \quad (67)$$

where, the superscript denotes the order to convolution.

Stationary probabilities  $Q_{n_1, n_2}(r)$  that the system is in the state  $(n_1, n_2, r) \in \Psi$  are defined as

$$Q_{n_1, n_2}(r) = \lim_{t \rightarrow \infty} P\{\xi_1(t) = n_1, \xi_2(t) = n_2, \delta(t) = r\}. \quad (68)$$

Consider the amount of resources that a session releases upon departure. Denote by  $\beta_{0,j}(n_1, n_2, r)$  the probability that,  $j$  resources are released as a result of the primary session departure provided that the system is in the state  $(n_1, n_2, r)$ . For  $r \leq R_0$ , the probabilities  $\beta_{0,j}(n_1, n_2, r)$  can be calculated using the Bayes law

$$\beta_{0,j}(n_1, n_2, r) = \frac{p_{0,j} \sum_{i=0}^{r-j} p_{0,i}^{(n_1-1)} p_{1,r-j-i}^{(n_2)}}{\sum_{i=0}^r p_{0,i}^{(n_1)} p_{1,r-i}^{(n_2)}}. \quad (69)$$

Similarly, define by  $\beta_{1,j}(n_1, n_2, r)$  the probability that as a result of the secondary session departure,  $j$  resources are released provided that the system is in the state  $(n_1, n_2, r)$ ,

$$\beta_{1,j}(n_1, n_2, r) = \frac{p_{1,j} \sum_{i=0}^{r-j} p_{0,i}^{(n_1)} p_{1,r-j-i}^{(n_2-1)}}{\sum_{i=0}^r p_{0,i}^{(n_1)} p_{1,r-i}^{(n_2)}}. \quad (70)$$

In the case of  $r > R_0$ , estimation of  $\beta_{0,j}(n_1, n_2, r)$  and  $\beta_{1,j}(n_1, n_2, r)$  is complicated as these probabilities depend on the arrival order of primary and secondary sessions, which cannot be determined from the state of the process. However, since the arrivals of the primary and secondary sessions are independent of each other and taking into account the known number of sessions of each type, any permutation of them in terms of the arrival time is equiprobable. Thus, the probability that the latest primary session takes the  $k$ -th place is

$$\binom{k-1}{n_1-1} / \binom{n_1+n_2}{n_1}, \quad (71)$$

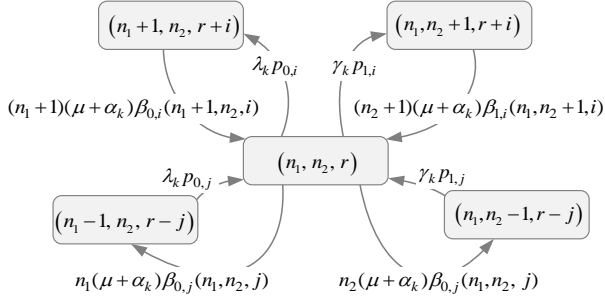


Fig. 17. Typical set of states and associated transition intensities.

where  $\binom{k-1}{n_1-1}$  is the number of ways to place  $n_1 - 1$  the primary session in the first  $k - 1$  places (since the last one will take the  $k$ -th place), and  $\binom{n_1+n_2}{n_1}$  is the overall number of ways to place  $n_1$  primary sessions. The probability that  $n_1$  primary sessions and  $k - n_1$  secondary sessions occupy  $i \leq R_0$  is calculated using the convolution

$$\sum_{s=0}^i p_{0,s}^{(n_1)} p_{1,i-s}^{(k-n_1)}, \quad (72)$$

Further, the probability that  $n_1$  primary and  $n_2$  secondary sessions occupy  $r$  resources, provided that the latest primary session takes the  $k$ -th place, is estimated as

$$\sum_{i=0}^{\min(r, R_0)} p_{1,r-i}^{(n_2+n_1-k)} \sum_{s=0}^i p_{0,s}^{(n_1)} p_{1,i-s}^{(k-n_1)}. \quad (73)$$

Finally, the probability that  $n_1$  primary and  $n_2$  secondary sessions together occupy  $r$  resources has the following form

$$\sum_{k=n_1}^{n_1+n_2} \frac{\binom{k-1}{n_1-1}}{\binom{n_1+n_2}{n_1}} \sum_{i=0}^{\min(r, R_0)} p_{1,r-i}^{(n_2+n_1-k)} \sum_{s=0}^i p_{0,s}^{(n_1)} p_{1,i-s}^{(k-n_1)}. \quad (74)$$

Estimation of  $\beta_{0,j}(n_1, n_2, r)$  and  $\beta_{1,j}(n_1, n_2, r)$  in the case  $r > R_0$  is not an easy computational problem. To reduce the computational complexity, one may utilize approximation obtained by neglecting the order of session arrivals, i.e.,

$$\beta_{0,j}(n_1, n_2, r) = \frac{p_{0,j} \sum_{i=0}^{\min(r-j, R_0-j)} p_{0,i}^{(n_1-1)} p_{1,r-j-i}^{(n_2)}}{\sum_{i=0}^{\min(r, R_0)} p_{0,i}^{(n_1)} p_{1,r-i}^{(n_2)}},$$

$$\beta_{1,j}(n_1, n_2, r) = \frac{p_{1,j} \sum_{i=0}^{\min(r-j, R_0)} p_{0,i}^{(n_1)} p_{1,r-j-i}^{(n_2-1)}}{\sum_{i=0}^{\min(r, R_0)} p_{0,i}^{(n_1)} p_{1,r-i}^{(n_2)}}. \quad (75)$$

By utilizing  $\beta_{0,j}(n_1, n_2, r)$  and  $\beta_{1,j}(n_1, n_2, r)$  the system of equilibrium equations for the process  $X(t)$  takes the form of (76). The typical subset of states and associated transition intensities are illustrated in Fig. 17.

3) *Performance Metrics*: The system of equilibrium equations defined in (76) needs to be solved numerically. Due to the fact that the number of equations in the system can reach  $N(N+1)R_1/2$ , we recommend using special libraries for

sparse matrices and associated iterative methods, i.e., Gauss-Seidel method [169], [170].

Once the stationary state distribution is obtained, performance metrics immediately follow. The new session drop probability  $\pi_{b,k}$  at BS  $k$  and the probability  $\pi_{s,k}$  that rerouting leads to the drop of a session take the form

$$\pi_{b,k} = 1 - \sum_{0 \leq n_1+n_2 \leq N-1} \sum_{r \leq R_{0,k}: (n_1, n_2, r) \in \Psi_{n_1, n_2}} Q_{n_1, n_2}(r) \sum_{j=0}^{R_{0,k}-r} p_{0,j},$$

$$\pi_{s,k} = 1 - \sum_{0 \leq n_1+n_2 \leq N-1} \sum_{r: (n_1, n_2, r) \in \Psi_{n_1, n_2}} Q_{n_1, n_2}(r) \sum_{j=0}^{R_{1,k}-r} p_{1,j}. \quad (77)$$

The intensities of secondary sessions are given by

$$\varphi_k = \sum_{v=1}^{\infty} \varphi_k^v,$$

$$\varphi_k^1 = \sum_{i=1}^K \lambda_i (1 - \pi_{b,i}) \frac{\alpha_i}{\mu + \alpha_i} \varphi_{i,k}^0,$$

$$\varphi_k^v = \sum_{i=1}^K \varphi_i^{v-1} (1 - \pi_{s,i}) \frac{\alpha_i}{\mu + \alpha_i} \varphi_{i,k}^{v-1}, \quad v > 1, \quad (78)$$

where  $v$  denotes the level of the secondary session.

The network-wide counterparts of these metrics are

$$\pi_b = \sum_{k=1}^K \frac{\lambda_k}{\lambda} \pi_{b,k}, \quad \pi_s = \sum_{k=1}^K \frac{\varphi_k}{\varphi} \pi_{s,k}, \quad (79)$$

and they need to be utilized as shown in Fig. 16.

Finally, the probability that the initially accepted for service session is eventually dropped is given by

$$\pi_O = \lim_{t \rightarrow \infty} \frac{\varphi \pi_s t}{\lambda(1 - \pi_b)t} = \frac{\varphi \pi_s}{\lambda(1 - \pi_b)}, \quad (80)$$

where the numerator is the mean number of accepted sessions that have been dropped during time  $t$ , and the denominator is the overall number of accepted sessions during time  $t$ .

4) *Illustrative Example*: The new and ongoing session drop probabilities in presence multiconnectivity obtained using the framework discussed above are shown in Fig. 18 for the session rate of 10 Mbps. Following [54] we consider a circular deployment with a number of BSs evenly spaced over the circumference. As one may observe, increasing the degree of multiconnectivity leads to the dramatic reduction in both new and ongoing session drop probability. This is in contrast to resource reservation that improves ongoing session drop probability at the expense of new session loss probability inducing a trade-off between these two metrics. However, this gain comes at the expense of increased implementation complexity, signaling load and the decreased energy efficiency of UEs. On top of this, the efficient use of this functionality requires dense mmWave BS deployments that are only feasible at later stages of 5G rollouts. Using the described framework one may also capture the joint effects of resource reservation and multiconnectivity. For in-depth analysis of this scenario we refer to [54].

$$\begin{aligned}
\text{(i)} \quad Q_0 \left[ \lambda_k \sum_{j=0}^{R_0} p_{0,j} + \varphi_k \sum_{j=0}^{R_1} p_{1,j} \right] &= (\mu + \alpha_k) \left[ \sum_{j:(1,0,j) \in \Psi_{1,0}} Q_{1,0}(j) + \sum_{j:(0,1,j) \in \Psi_{0,1}} Q_{0,1}(j) \right], \\
\text{(ii)} \quad Q_{n_1, n_2}(r) \left[ \lambda_k \sum_{j=0}^{R_0-r} p_{0,j} + \varphi_k \sum_{j=0}^{R_1-r} p_{1,j} + (n_1 + n_2)(\mu + \alpha_k) \right] &= \lambda_k \sum_{j:(n_1-1, n_2, r-j) \in \Psi_{n_1-1, n_2}} p_{0,j} Q_{n_1-1, n_2}(r-j) + \\
&+ \varphi_k \sum_{j:(n_1, n_2-1, r-j) \in \Psi_{n_1, n_2-1}} p_{1,j} Q_{n_1, n_2-1}(r-j) + (n_1 + 1)(\mu + \alpha_k) \sum_{j:(n_1+1, n_2, r+j) \in \Psi_{n_1+1, n_2}} Q_{n_1+1, n_2}(r+j) \beta_{0,j}(n_1 + 1, n_2, r+j) + \\
&+ (n_2 + 1)(\mu + \alpha_k) \sum_{j:(n_1, n_2+1, r+j) \in \Psi_{n_1, n_2+1}} Q_{n_1, n_2+1}(r+j) \beta_{1,j}(n_1, n_2 + 1, r+j), \quad n_1 + n_2 < N, r \leq R_0, \\
\text{(iii)} \quad Q_{n_1, n_2}(r) \left[ \varphi_k \sum_{j=0}^{R_1-r} p_{1,j} + (n_1 + n_2)(\mu + \alpha_k) \right] &= \varphi_k \sum_{j:(n_1, n_2-1, r-j) \in \Psi_{n_1, n_2-1}(r-j)} p_{1,j} Q_{n_1, n_2-1}(r-j) + \\
&+ (n_1 + 1)(\mu + \alpha_k) \sum_{j:(n_1+1, n_2, r+j) \in \Psi_{n_1+1, n_2}} Q_{n_1+1, n_2}(r+j) \beta_{0,j}(n_1 + 1, n_2, r+j) + \\
&+ (n_2 + 1)(\mu + \alpha_k) \sum_{j:(n_1, n_2+1, r+j) \in \Psi_{n_1, n_2+1}} Q_{n_1, n_2+1}(r+j) \beta_{1,j}(n_1, n_2 + 1, r+j), \quad n_1 + n_2 < N, r > R_0, \\
\text{(iv)} \quad (n_1 + n_2)(\mu + \alpha_k) Q_{n_1, n_2}(r) &= \\
&= \lambda_k \sum_{j:(n_1-1, n_2, r-j) \in \Psi_{n_1-1, n_2}} p_{0,j} Q_{n_1-1, n_2}(r-j) + \varphi_k \sum_{j:(n_1, n_2-1, r-j) \in \Psi_{n_1, n_2-1}} p_{1,j} Q_{n_1, n_2-1}(r-j), \quad n_1 + n_2 = N, r \leq R_0. \\
\text{(v)} \quad (n_1 + n_2)(\mu + \alpha_k) Q_{n_1, n_2}(r) &= \varphi_k \sum_{j:(n_1, n_2-1, r-j) \in \Psi_{n_1, n_2-1}} p_{1,j} Q_{n_1, n_2-1}(r-j), \quad n_1 + n_2 = N, r > R_0.
\end{aligned} \tag{76}$$

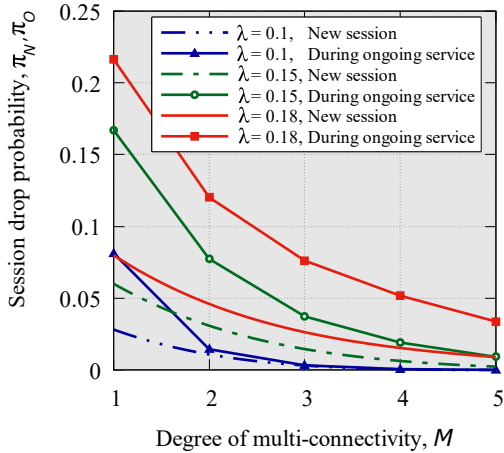


Fig. 18. New and ongoing session drop probabilities.

### F. Multiple Flows with Priorities

Finally, we consider how to incorporate session priorities in the considered framework. To this aim, consider a resource queuing system with two types of sessions, (e.g., URLLC and eMBB), preemptive priority service discipline,  $N$  servers and resource volume  $R$ . Here, we refer to prioritized sessions as first type sessions. Other sessions are referred to as second

type sessions. Both types of sessions arrive according to mutually independent Poisson processes with parameters  $\lambda_1$  and  $\lambda_2$ , respectively, and their service times are exponentially distributed with intensities  $\mu_1$  and  $\mu_2$ . Besides, the resource requirements distributions are  $\{p_{1,r}\}$  and  $\{p_{2,r}\}$ ,  $r \geq 0$ .

The behavior of the considered system can be described by four-dimensional Markov process  $(\xi_1(t), \delta_1(t), \xi_2(t), \delta_2(t))$ , where  $\xi_i(t)$  is the number of  $i$ -th type sessions in the system and  $\delta_i(t)$  is the total number of resources occupied by  $i$ -th type sessions at time  $t$ . However, the straightforward approach to obtain steady-state distribution of the number of sessions via numerical solution of the system of equilibrium equations is not feasible. The reason is the state space explosion with the number of states reaching  $(N+1)(N+2)(R+1)(R+2)/4$ . To decrease computational complexity of the solution, one may resort to the approximation by deducing performance metrics via marginal distributions of both type of sessions in the system. To demonstrate the basic principles, denote by  $Q_i(n_i, r_i)$  the marginal distribution that  $n_i$ ,  $i = 1, 2$ , sessions of  $i$ th type totally occupy  $r_i$  resources. Observe that under the preemptive priority service discipline, the service process of the first type of sessions is not affected by the service process of the second type of sessions. Thus, the marginal distribution  $Q_1(n_1, r_1)$  can be obtained by solving (40) for the system with only first type of sessions.

To determine  $Q_2(n_2, r_2)$  knowing  $Q_1(n_1, r_1)$  one may utilize the following idea. Observe that when there are  $n_2$  second type sessions that totally occupy  $r_2$  resources, the number of priority sessions and resources occupied by them is given by the marginal distribution  $Q_1(n_1, r_1)$  given that there are no more than  $N - n_2$  of them, and they totally occupy no more than  $R - r_2$  resources. Applying this idea, one can estimate the following auxiliary probabilities that depend on the number of second type sessions in the system and volume of resources occupied by them: (i) the probability that an arriving session of the second type is dropped and (ii) the probability that an arriving session of the first type interrupts the service process of  $k$  sessions of the second type. With these probabilities in hand, one may further derive the system of equilibrium equations for the marginal distribution  $Q_2(n_2, r_2)$ , which is then solved numerically. The performance metrics of interest including drop probabilities of both types of sessions as well as the probability that session of the second type will be interrupted during the service will immediately follow.

1) *Illustrative Example:* The described framework has been applied in [171] to evaluate priority-based service between URLLC and eMBB sessions served as mmWave BS. We consider a single cell system with session arrivals governed by the Poisson process whose geometric locations are uniformly distributed in the cell service area. We illustrate high-priority and low-priority session drop probabilities as well as low-priority session interruption probability in Fig. 19 as a function of high-priority session arrival intensity  $\lambda_1$ . As expected the high-priority traffic, e.g., URLLC, is well-isolated from the low-priority one. However, there is a complex interplay between low-priority session drop probability and session interruption probability, where the latter first decreases and then, starting from  $\lambda_1 \approx 17$  sessions/s, increases. To reduce the latter undesirable effect of dropping sessions already accepted to service one may apply resource reservation for low-priority traffic. This type of system can also be analyzed within the proposed framework by combining the priority model with the resource reservation model considered above. Note that priority service, and thus, the proposed framework can also be applied to enable slicing at the air interface [65], [67].

## V. RADIO ABSTRACTION AND PARAMETERIZATION

In this section, we outline the basic techniques for parameterizing the models introduced in the previous section. Recall that the queuing part accepts the following parameters as the input: the pmf of the amount of requested resources,  $\{p_j\}_{j \geq 0}$ , and the temporal intensity of the UE stage changes,  $\alpha$ . These parameters abstract the propagation and antenna specifics, UE locations, blockage and micromobility and represent them in the form suitable for queuing analysis. Below, we first specify the parameterization procedure in detail for the baseline model having PPP deployment of mmWave/THz BSs and UEs randomly located in the BS coverage area. Whenever possible we also sketch the extension for other deployment cases.

### A. Resource Request Characterization

For certainty, consider propagation model defined in Section III excluding the exponential component responsible for

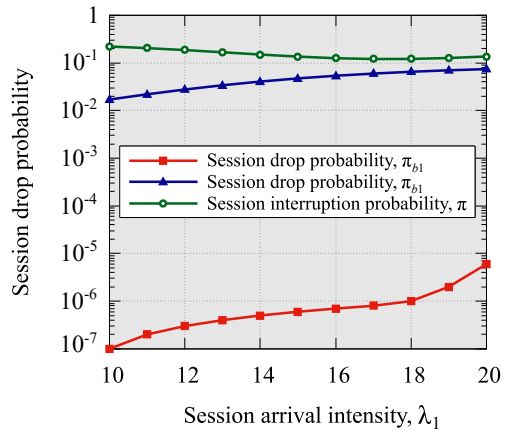


Fig. 19. Performance metrics for prioritized service at BSs.

atmospheric absorption. To derive the pmf of the amount of requested resources, we start with SINR at the UE located at the distance of  $y$  from the mmWave/THz along the propagation path is provided by

$$S(y) = \frac{C}{N_0 + I} [y^{-\zeta_1} [1 - p_B(y)] + y^{-\zeta_2} p_B(y)], \quad (81)$$

where  $C = P_A G_A G_U / A$ ,  $P_A$  is the BS transmit power,  $G_A$  and  $G_U$  are the antenna array gains at the BS and UE sides, respectively,  $N_0$  is the thermal noise,  $I$  is the interference,  $A$ ,  $\zeta_1$  and  $\zeta_2$  are the propagation coefficients provided in (3).

There is a single unknown to determine in (81), the interference,  $I$ . Observe that this is a RV that depends on the plethora of deployment factors including BS deployment model, utilized antenna arrays, emitted power, the density of blockers, etc. For a given deployment scenario, interference can be estimated by utilizing conventional stochastic geometry approaches, e.g., [75], [74], [172], [45], [173], [173]. Finally, if one wants to account for more detailed propagation specifics, e.g. fast and shadow fading, these can also be added to the numerator of (81). For example, shadow fading distribution is known to follow Normal distribution with zero mean and standard deviation that can be found in [90].

Analyzing the structure of (81) one may observe that coefficients  $P_A$ ,  $G_A$ ,  $G_U$ ,  $N_0$  are all constants. The blockage probability  $p_B(y)$  can be derived utilizing the blockage models specified in (5). On the other hand, the distance between UE and BS,  $y$ , interference,  $I$  as well as additional components such as shadow fading and fast fading are all RVs. The presence of multiple RVs drastically complicates the derivation of pmf of resources requested by a session as shown in [174], [175], [75]. Thus, to simplify derivations, interference is often captured by an interference margin corresponding to the mean value in a given deployment of interest. In what follows, we illustrate how to derive the mean value of interference when the fast fading component is neglected while the shadow fading is captured by the shadow fading margin.

1) *Interference Characterization*: For a considered deployment,  $I$ , the interference can be written as

$$I = \sum_{i=1}^N C(y_i^{-\zeta_1} [1 - p_B(y_i)] + y_i^{-\zeta_2} p_B(y_i)), \quad (82)$$

where  $Y_i$  are the distances to interfering BS.

Observe, that interference in (82) is a random function of RVs. Unfortunately, there are no effective methods to derive its distribution. For dense deployments, however, one may approximate it utilizing the Normal distribution. Alternatively, when approximating interference in (81), one may utilize the mean values of interference as an interference margin. The latter can be obtained by applying the Campbell theorem expressing the moments of aggregated interference at a randomly selected (tagged) UE as follows [176]

$$E[I^n] = \int_0^{r_I} C[x^{-\zeta_1}(1 - p_B(x)) + x^{-\zeta_2} p_B(x)]^n \times p_C(x) 2\xi\pi x dx, \quad (83)$$

where  $2\xi\pi x dx$  is the probability that there is BS in the radius increment of  $dx$ ,  $p_C(x)$  is the so-called exposure probability, that is, the probability that the antennas of interfering BSs are oriented towards the considered UE, and  $p_B(x)$  is the blockage probability at the distance  $x$ ,  $r_I$  is the maximum radius, where BSs contribute non-negligible interference at the tagged UE.

The only unknown component in (83) is the exposure probability,  $p_C(x)$ . For 2D deployments or when the vertical directivity is much smaller compared to the horizontal one, one may determine it following [45] as

$$p_C(x) = p_C = \alpha_A \alpha_U / 4\pi^2, \quad (84)$$

where  $\alpha_A$  and  $\alpha_U$  are HPBW angles of antennas at BS and UE sides. These parameters can be estimated as a function of the number of antenna elements and the type of utilized antenna model as discussed in Section III. For 3D radiation patterns the exposure probability  $p_C$  has a more complex structure but can still be obtained in closed-form as shown in [75].

2) *SINR Distribution*: Recall that the distance from BS to UE uniformly distributed over the circularly shaped area is given by pdf in the form of  $f_Y(y) = 2y/r_E^2$ ,  $0 < y < r_E$ , where  $r_E$  is the BS coverage radius. Observe, that depending on the density of BS in the environment the effective coverage radius,  $r_E$ , can be limited by SINR (sparse deployments) or by cell boundaries (dense deployments). This, in turn, affects the distribution of UE locations in the cell and, the received signal strength, and SINR. Thus, the coverage radius,  $r_E$ , is determined by two distances – inter-BS distance,  $r_{E,V}$ , and the maximum coverage of BSs,  $r_{E,S}$ , i.e.,  $r_E = \min(r_{E,V}, r_{E,S})$ . The latter can be obtained by determining the maximum distance between the UE and the BS, such that the UE in the LoS blocked conditions is not in the outage state. By utilizing the propagation model defined in Section III the sought 2D distance  $r_{E,S}$  can be written as

$$S = C (r_{E,S}^2 + (h_A - h_U)^2)^{-\frac{\zeta_2}{2}} = S_{th}, \quad (85)$$

where  $S_{th}$  is the SINR threshold associated with the worst possible MCS defined for a given technology, e.g., see [153] for mmWave NR,  $h_A$  is the BS height,  $h_U$  is the UE height.

Solving for  $r_{E,S}$ , we obtain

$$r_{E,S} = \sqrt{(C/S_{th})^{\frac{2}{\zeta_2}} - (h_A - h_U)^2}. \quad (86)$$

The second component – inter-BS distance,  $r_{E,V}$  heavily depends on the type of deployment. For hexagonal cellular deployments with tri-sector antenna BS it is specified by  $D = 3R$  [177], where  $R$  is the radius of a cell. For semi-regular deployments considered in Section III it is defined by the scenario geometry. Finally, for random deployments, one may obtain the sought radius by determining the half distance between typical BS locations. For the PPP field of BSs, the BS coverage area is known to form Voronoi cells. Thus, one may approximate it by the circle with the corresponding mean area. Since there is no analytical expression for the area of a Voronoi cell, one needs to resort to computer simulations or utilize approximations available in, e.g., [178], [179].

Once the pdf of the distance to the tagged UE,  $f_Y(y) = 2y/r_E^2$ ,  $0 < y < r_E$ , as well as interference margin (83) are both determined, one can proceed with characterizing SINR distribution. The impact of the shadow fading can also be accounted by utilizing the constant shadow fading margins,  $M_{S,i}$  for the LoS non-blocked and blocked states, i.e.,

$$M_{S,i} = \sqrt{2}\sigma_{S,i}, \quad (87)$$

where  $\sigma_{S,i}$  is the standard deviations of the shadow fading distribution in LoS non-blocked and blocked states provided in [90]. Then, the SINR CDF can be obtained using RV transformation technique as a function of a single RV – distance from UE to BS as described in [180].

To illustrate the derivations, let  $S_{nB}$  be a RV denoting the SINR in non-blocked state and  $F_{S_{nB}}(x)$ ,  $x > 0$ , be its CDF. Since UEs are assumed to uniformly distributed in the circularly shaped BS coverage, the CDF of the distance between UE and BS can be obtained as

$$F_Y(y) = (y^2 - (h_A - h_U)^2)/r_E^2, \quad (88)$$

where  $y \in (|h_A - h_U|, \sqrt{r_E^2 + (h_A - h_U)^2})$ .

Observe that SINR is a monotonously decreasing function of distance  $y$ . Thus, the CDF of SINR can be expressed as

$$F_{S_{nB}}(y) = 1 - F_Y(C/(N_0 + I)y^{\zeta_1/2}). \quad (89)$$

One may utilize the described technique to obtain SINR distribution for the blocked state. Further, if one wants to include the effect of the shadow fading distribution the following step needs to be performed. Specifically, let  $F_{S_{nB}}^{dB}(y) = F_{S_{nB}}(10y/10)$  be CDF of SINR in dB scale. Recall that shadow fading is known to follow Log-Normal distribution in linear scale resulting in Normal distribution in dB scale. By utilizing these observations, the SINR distribution in non-blocked state can be written as

$$S_{nB,S}^{dB} = S_{nB}^{dB} + N(0, \sigma_{S,nB}), \quad (91)$$

where  $N(0, \sigma_{S,nB})$  is the Normal distribution with zero mean and standard deviation  $\sigma_{S,nB}$  specifying shadow fading.



$$\begin{aligned}
F_{S_{nB}^{dB}}(y) = & \frac{1}{2r_E^2} \left[ A^{2/\zeta_1} 10^{-\frac{y}{5\zeta_1}} e^{\frac{\sigma_{S,nB}^2 \log^2(10)}{50\zeta_1^2}} \left[ \operatorname{erf} \left( \frac{50\zeta_1 \log(A) - 25\zeta_1^2 \log(r_E^2 + (h_A - h_U)^2) + \sigma_{S,nB}^2 \log^2(10) - 5\zeta_1 y \log(10)}{5\sqrt{2}\zeta_1 \sigma_{S,nB} \log(10)} \right) \right. \right. \\
& - \operatorname{erf} \left( \frac{50\zeta_1 (\log(A) - \zeta_1 \log(h_A - h_U)) + \sigma_{S,nB}^2 \log^2(10) - 5\zeta_1 y \log(10)}{5\sqrt{2}\zeta_1 \sigma_{S,nB} \log(10)} \right) \left. \right] + (r_E^2 + (h_A - h_U)^2) \times \\
& \times \operatorname{erf} \left( \frac{-10 \log(A) + 5\zeta_1 \log(r_E^2 + (h_A - h_U)^2) + y \log(10)}{\sqrt{2}\sigma_{S,nB} \log(10)} \right) - (h_A - h_U)^2 \times \\
& \times \operatorname{erf} \left( \frac{\sqrt{2}(-10 \log(A) + 10\zeta_1 \log(h_A - h_U) + y \log(10))}{\sigma_{S,nB} \log(100)} \right) + r_E^2 \left. \right]. \quad (90)
\end{aligned}$$

Finally, the SINR CDF accounting for both path loss and shadow fading can be obtained as a sum of two RVs, that is, by convolving  $F_{S_{nB}^{dB}}(y)$  and  $N(0, \sigma_S)$ , immediately leading to

$$F_{S_{nB,S}^{dB}}(y) = \int_{-\infty}^{\infty} F_{S_{nB}^{dB}}(y+u) \frac{e^{-u^2/2\sigma_S^2}}{\sqrt{2\pi}\sigma_S} du. \quad (92)$$

Unfortunately, no closed-form expression for 92 can be obtained by utilizing the conventional RV transformation technique [180]. However, one may still obtain the final results in terms of an error function,  $\operatorname{erf}(\cdot)$ , as provided in (90), where

$$A = \frac{P_A 10^{G_A G_U / 10}}{f_c^2 10^{3.24 + L_B / 10} 10^{\frac{1}{10}(M_{S,1})} N_0}, \quad (93)$$

$M_{S,1}$  is the interference margin,  $L_B$  is the additional losses induced by the blockage. By weighting SINR CDFs corresponding to LoS blocked and non-blocked states with probabilities  $p_B$  and  $(1 - p_B)$  one obtains the final result. Finally, we note that  $p_B$  – the averaged blockage probability, can be estimated as follows

$$\pi_B = \int_0^{r_E} p_B(x) \frac{2x}{r_E^2} dx, \quad (94)$$

where  $p_B(x)$  is available from (5). The authors in [181] demonstrated that the resulting SINR CDF can be well approximated by Normal distribution.

3) *Resource Request Distributions*: To determine resource request distribution we now introduce SINR thresholds corresponding to MCS schemes,  $S_j$ ,  $j = 1, 2, \dots, J$ . Further, we define the probability that UE is assigned MCS  $j$  by  $\epsilon_j$ . By discretizing SINR CDF  $F_S(s)$ , we obtain

$$\begin{cases} \epsilon_0 = F_S(S_1), \\ \epsilon_j = F_S(S_{j+1}) - F_S(S_j), \quad j = 1, 2, \dots, J-1, \\ \epsilon_J = 1 - F_S(S_J). \end{cases} \quad (95)$$

The probability  $\epsilon_j$  that a session requests  $r_j$  RBs can now be used to determine the resource requirements of sessions characterized by a certain requested rate. Note that the latter can be fixed or random depending on the considered scenario.

4) *Usage of 3D Cluster-Based Propagation Model*: One may characterize the resource request distribution more precisely by utilizing 3D cluster-based propagation model as discussed in [154]. Here, the most complex part is the derivation of the pdf of the received power at a distance  $x$  from BS.

Assuming that UE always utilizes the strongest cluster the sought pdf is provided by

$$f_{P_R}(z; x) = \sum_{i=1}^W \left[ (1 - p_{B,i}(x)) \prod_{j=1}^{i-1} p_{B,j}(x) \right] f_{P_n}(z; x), \quad (96)$$

$p_{B,i}(x)$  is the cluster blockage probability at distance  $x$ ,  $f_{P_n}(z; x)$  is the pdf of power of cluster  $n$  at the distance  $x$ . The latter parameters is obtained by utilizing RV transformation technique as follows [180]

$$f_{P_n}(z; x) = \frac{f_{P_{s,n}} \left( \frac{P_n(x)}{10^{[P_A - L_{dB}(x)]/10}} \right)}{10^{[P_A - L_{dB}(x)]/10}}, \quad (97)$$

where  $L_{dB}(x)$  is the pass loss in dB,  $f_{P_{s,n}}$  is provided in (10).

Integrating (96) over the cell radius one obtains

$$f_{P_R}(z) = \int_0^{r_E} f_{P_R}(z; x) \frac{2x}{r_E^2} dx. \quad (98)$$

The other unknowns in (96) are the cluster blockage probabilities at distance  $x$ ,  $p_{B,i}(x)$ . Here, the LoS cluster blockage is obtained similarly to (5). However, to estimate probabilities  $p_{B,i}$ ,  $i = 2, 3, \dots$  one needs ZoA pdf,  $f_{\theta_i}(y; x)$ , provided in (10). Particularly, following [99], the cluster  $i$ ,  $i = 2, 3, \dots, N$ , blockage probability conditioned on ZoA  $y_i$  is given by

$$p_{B,i}(y; x) = 1 - e^{-2\lambda_B r_B (\tan y_i (h_B - h_U) + r_B)}. \quad (99)$$

leading to the cluster blockage probability in the form of

$$p_{B,i}(x) = \int_{-\pi}^{\pi} f_{\theta_i}(y; x) p_{B,i}(y; x) dy, \quad (100)$$

which can be estimated by numerical integration.

By using  $p_{B,i}$ ,  $i = 1, 2, \dots, N$  one may also obtain outage probability required in those deployments, where blockage leads to outage conditions as shown in [99]

$$p_O(x) = \prod_{i=1}^N p_{B,i}(x) + \int_0^{S_T} f_{P_R}(z; x) dz, \quad (101)$$

where  $S_T$  is the UE sensitivity threshold.

For complex scenario geometries and/or service rules involving a field of BS and multiconnectivity one may further extend the baseline parameterization models. Particularly, the case of multiconnectivity in square mmWave BS deployments with multiconnectivity operation is considered in [54].

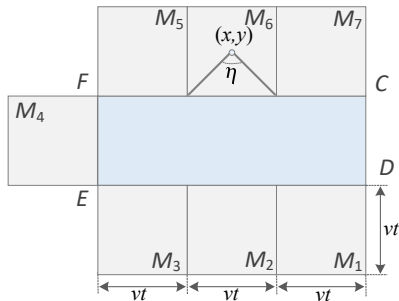


Fig. 20. Translation of spatial blocker intensity into temporal domain.

### B. UE State Changes

There are two critical impairments that may affect session continuity of applications served by mmWave or THz systems – micromobility and blockage. In the presented framework both can be abstracted using the external Poisson process of “signals” associated with sessions currently served at BSs. Below, we first characterize UE state changes caused by micromobility process and then proceed describing state changes induced by dynamic blockage phenomenon. We also specifically note that the queuing framework assumes only one type of impairment to be taken into account. However, it can be extended to the case of more than a single external process associated with sessions. Finally, notice that the Poisson nature of state changes also limits the modeling capabilities to mean values of the state holding times. Extending the framework to more complex external signal patterns is more complicated.

1) *State Changes due to Micromobility:* Consider first the process of UE state changes caused by micromobility of UE. Here, UE transitions between “connectivity” and outage states. The duration of both states heavily depends on the considered beamsearching strategy, i.e., on the time instant, when beamsearching is initiated. Let  $T_C$  and  $T_O$  be RVs denoting connectivity and outage time, respectively. In the simplest “on-demand” beamsearching scheme, where beamsearching is invoked when the connection is lost the pdf of the connectivity time  $f_{T_C}(t)$  coincides with the time to outage  $f_{T_A}(t)$  provided in [19] and given in (20) while the outage time,  $T_O$  coincides with the duration of the beamsearching procedure,  $T_B$ , discussed in Section III. Note that the latter is affected by the utilized beamsearching algorithm and, generally, depends on the number of antenna elements and array switching time.

Another type of the beamalignment strategy is periodic alignment. Here, beam realignment procedure runs regularly with a period  $T_U$ . Note that this scheme reflects the cellular-style system design with centralized control, while the former “on-demand” one is characteristic for WLANs. Here, the connectivity time can be determined as the minimum of  $T_A$  provided in (20) and constant  $T_U$ , i.e.,

$$f_{T_C}(t) = \begin{cases} f_{T_A}(t), & T_A < T_U \\ f_{T_A}(t) / \int_0^{T_U} f_{T_A}(x) dx, & T_A \geq T_U \end{cases}, \quad (102)$$

while the outage time again coincides with  $T_B$ .

2) *State Changes due to Blockage:* Consider now temporal dynamics of the blockage process. For illustrative purposes,

we consider only one dynamic blockage model introduced in Section III, where UE is assumed to be static in a field of human blockers with density  $\lambda_B$  moving according to RDM [120]. Particularly, we are interested in the mean duration of blocked and non-blocked intervals. Similar derivations can be performed for other dynamic models.

We start by determining the intensity of blockers entering the LoS blockage zone of UE located at the distance  $x$  from BS,  $\epsilon(x)$ . To this aim, we draw an area around the LoS blockage zone and divide it into  $i$ ,  $i = 1, 2, \dots, 7$  sub-zones as shown in Fig. 20. Now, the generic expression binding the density of blockers in the environment with the temporal intensity of blockers entering the LoS blockage zone is

$$\epsilon(x) = \sum_{i=1}^7 \iint_{M_i} g_i(x, y) Pr\{E\} Pr\{T > 1\} \lambda_B M_i dx dy, \quad (103)$$

where  $M_i$  is the area of zone  $i$ ,  $g_i(x, y)$  is the pdf of blockers locations in sub-zone  $i$  provided by  $g_i(x, y) = 1/M_i$ ,  $E$  is the event that blockers move towards the LoS blockage zone, and  $Pr\{T > 1\} = \exp(-1/\tau)$  is the probability that a blocker moves longer than a unit time without changing the movement direction. The unknown event,  $E$ , can be obtained by considering that there is a range of angles leading to the blocker hitting the LoS blockage zone  $\eta_i(x, y)$ . That is,  $Pr\{E\} = \eta_i(x, y)/2\pi$ . With these observations in hand, we may rewrite (103) as follows

$$\epsilon(x) = \frac{\lambda_B e^{-1/\tau}}{2\pi} \sum_{i=1}^7 \iint_{M_i} \eta_i(x, y) dx dy, \quad (104)$$

where ranges of movements,  $\eta_i(x, y)$ , can be estimated as

$$\begin{aligned} \eta_1(x, y) &= ([x_D - x]/vt), \quad i = 1, 3, 5, 7, \\ \eta_2(x, y) &= 2 \cos^{-1}([x_E - x]/vt), \quad i = 2, 6, \\ \eta_4(x, y) &= 2 \tan^{-1}([x - x_E]/[y - y_E]), \end{aligned} \quad (105)$$

where  $x_{(\cdot)}, y_{(\cdot)}$  are the coordinates in Fig. 20. Finally, the mean intensity of blockers crossing LoS blockage zone is

$$\epsilon = \int_0^{r_E} \epsilon(x) 2x/r_E^2 dx, \quad (106)$$

where  $r_E$  is the BS service radius.

Alternatively to the described method, one may utilize the result of [182] revealing that the inter-meeting time between a point moving according to RDM in a certain convex region  $A$  and a static convex region  $A_1 \subset A$  is approximately exponentially distributed. The parameter of exponential distribution depends on the areas of  $A$ ,  $A_1$  and the speed of a moving point. This implies that the process of meetings is Poisson in nature. By utilizing the superposition property of the Poisson process [183] one may determine the temporal intensity of blockers crossing the LoS blockage zone.

To proceed further, we recall that the blockage process at UE is known to have an alternative renewal structure [24]. In the same study the authors also demonstrated that under Poisson assumption of blockers entering the LoS blockage area the non-blocked interval follows exponential distribution parameter coinciding with the intensity of the Poisson process.

$$F_\eta(x) = 1 - \left[ 1 - F_{T_B}(x) \right] \left[ 1 - \int_0^x (1 - F_\eta(x-z)) \exp(-\lambda_{B,T} F_{T_B}(z)) \lambda_{B,T} dz \right] + \int_0^x (1 - F_\eta(x-z)) |de^{-\lambda_{B,T} F_{T_B}(z)}|. \quad (107)$$

In its turn, the blocked period may be formed by multiple blockers passing through the LoS blockage zone. By utilizing the analogy with the  $M/GI/\infty$  queuing system, the duration of the blocked interval is shown to coincide with the busy period distribution. This distribution can be calculated numerically by using the results of [121] provided in (107). The only unknown required is the distribution of the time it takes for a blocker to cross the LoS blockage zone. This can be found by assuming a random entrance point to the LoS blockage zone as shown in [24]. To simplify derivations, one may observe that the length of the LoS blockage zone is often significantly larger than its width. Thus, one may assume that blockers cross the LoS blockage zone following a direction perpendicular to its short side. In this case, the service time in the equivalent queuing model is deterministic and equals to  $2r_B/v$ , where  $r_B$  and  $v$  are the radius and speed of the blocker.

The intensity of state changes caused by blockage,  $\alpha$ , can be estimated by utilizing the mean blocked and non-blocked periods. Note that to avoid the complexity of estimating CDF in (107) one may resort to  $M/M/\infty$  approximation for which the mean busy period is available in closed form [184].

## VI. CONCLUSIONS

MmWave and THz communications systems are expected to build the foundation of future cellular access providing extreme amount of resources at the air interface. These systems are primarily targeted to support principally new applications such as AR/VR/XR, holographic telepresence, characterized by high bitrate non-elastic traffic patterns. However, intrinsic characteristics of mmWave and THz frequency bands such as extreme path losses, blockage, and micromobility makes provisioning of QoS guarantees to these applications an extremely complex task inherently requiring complex mechanisms to maintain session continuity.

In this paper, we provided a tutorial on mathematical analysis of mmWave and THz deployments with non-elastic traffic patterns. Particularly, we extended the conventional methods of stochastic geometry that are inherently limited to systems supporting elastic traffic only, to the case of composite models capturing both radio specifics of mmWave and THz bands as well as traffic service dynamics at BSs. These two parts of the composite framework are interrelated to each other via a well-defined interface parameters. On top of this, we also provided a comprehensive review of analytically tractable models of various components utilized for building the modeling scenarios including deployment, propagation, antenna, blockage, micromobility, beamsearching, traffic and service models under different system and environmental conditions.

The modular structure of the framework allows for a potential reuse of its core parts for studying various mmWave and THz deployments (including combinations of them) characterized by different scenario geometry, blocker types and their

mobility, antenna arrays, micromobility patterns of applications, network associations, reliability and rate improvement mechanisms. Finally, we considered several applications including systems with resource reservation, multiconnectivity, and priorities between arriving sessions.

## REFERENCES

- [1] M. Volk and J. Sterle, "5G Experimentation for Public Safety: Technologies, Facilities and Use Cases," *IEEE Access*, vol. 9, pp. 41 184–41 217, 2021.
- [2] J. Antoniou, "Quality of Experience and Emerging Technologies: Considering Features of 5G, IoT, Cloud and AI," in *Quality of Experience and Learning in Information Systems*. Springer, 2021, pp. 1–8.
- [3] S. Hutajulu, W. Dhewanto, and E. A. Prasetyo, "Two scenarios for 5G deployment in Indonesia," 2020.
- [4] V. Petrov, T. Kurner, and I. Hosako, "IEEE 802.15. 3d: First Standardization Efforts for Sub-Terahertz Band Communications toward 6G," *IEEE Communications Magazine*, vol. 58, no. 11, pp. 28–33, 2020.
- [5] M. Giordani, M. Polese, M. Mezzavilla, S. Rangan, and M. Zorzi, "Toward 6G networks: Use cases and technologies," *IEEE Communications Magazine*, vol. 58, no. 3, pp. 55–61, 2020.
- [6] M. Polese, J. M. Jornet, T. Melodia, and M. Zorzi, "Toward end-to-end, full-stack 6G terahertz networks," *IEEE Communications Magazine*, vol. 58, no. 11, pp. 48–54, 2020.
- [7] I. F. Akyildiz, J. M. Jornet, and C. Han, "Terahertz band: Next frontier for wireless communications," *Physical Communication*, vol. 12, pp. 16–32, 2014.
- [8] S. Parkvall, E. Dahlman, A. Furuskar, and M. Frenne, "Nr: The new 5g radio access technology," *IEEE Communications Standards Magazine*, vol. 1, no. 4, pp. 24–30, 2017.
- [9] J. G. Andrews, S. Buzzi, W. Choi, S. V. Hanly, A. Lozano, A. C. Soong, and J. C. Zhang, "What will 5G be?" *IEEE Journal on Selected Areas in Communications*, vol. 32, no. 6, pp. 1065–1082, 2014.
- [10] B. Sadhu, A. Paidimarri, M. Ferriss, M. Yeck, X. Gu, and A. Valdes-Garcia, "A 128-element dual-polarized software-defined phased array radio for mm-wave 5G experimentation," in *Proceedings of the 2nd ACM Workshop on Millimeter Wave Networks and Sensing Systems*. ACM, 2018, pp. 21–25.
- [11] I. F. Akyildiz and J. M. Jornet, "Realizing ultra-massive mimo (1024×1024) communication in the (0.06–10) terahertz band," *Nano Communication Networks*, vol. 8, pp. 46–54, 2016.
- [12] C. G. Ruiz, A. Pascual-Iserte, and O. Muñoz, "Analysis of Blocking in mmWave Cellular Systems: Characterization of the LOS and NLOS Intervals in Urban Scenarios," *IEEE Transactions on Vehicular Technology*, vol. 69, no. 12, pp. 16 247–16 252, 2020.
- [13] S. Mohebi, F. Michelinakis, A. Elmokashfi, O. Grøndalen, K. Mahmood, and A. Zanella, "Sectors, Beams and Environmental Impact on Commercial 5G mmWave Cell Coverage: an Empirical Study," *arXiv preprint arXiv:2104.06188*, 2021.
- [14] N. Tafintsev, D. Moltchanov, S. Andreev, S.-p. Yeh, N. Himayat, Y. Koucheryavy, and M. Valkama, "Handling Spontaneous Traffic Variations in 5G+ via Offloading Onto mmWave-Capable UAV Bridges," *IEEE Transactions on Vehicular Technology*, vol. 69, no. 9, pp. 10 070–10 084, 2020.
- [15] K. Haneda *et al.*, "5G 3GPP-like channel models for outdoor urban microcellular and macrocellular environments," in *IEEE 83rd Vehicular Technology Conference (VTC Spring)*, May 2016, pp. 1–7.
- [16] G. R. MacCartney, S. Deng, S. Sun, and T. S. Rappaport, "Millimeter-wave human blockage at 73 ghz with a simple double knife-edge diffraction model and extension for directional antennas," in *2016 IEEE 84th Vehicular Technology Conference (VTC-Fall)*. IEEE, 2016, pp. 1–6.
- [17] V. Petrov, D. Moltchanov, J. M. Jornet, and Y. Koucheryavy, "Exploiting multipath terahertz communications for physical layer security in beyond 5g networks," in *IEEE INFOCOM 2019-IEEE Conference on Computer Communications Workshops (INFOCOM WKSHPS)*. IEEE, 2019, pp. 865–872.

- [18] A. Orsino, D. Moltchanov, M. Gapeyenko, A. Samuylov, S. Andreev, L. Militano, G. Araniti, and Y. Koucheryavy, "Direct connection on the move: Characterization of user mobility in cellular-assisted d2d systems," *IEEE Vehicular Technology Magazine*, vol. 11, no. 3, pp. 38–48, 2016.
- [19] V. Petrov, D. Moltchanov, Y. Koucheryavy, and J. M. Jornet, "Capacity and outage of terahertz communications with user micro-mobility and beam misalignment," *IEEE Transactions on Vehicular Technology*, vol. 69, no. 6, pp. 6822–6827, 2020.
- [20] —, "The effect of small-scale mobility on terahertz band communications," in *Proceedings of the 5th ACM International Conference on Nanoscale Computing and Communication*, 2018, pp. 1–2.
- [21] S. K. Moorthy and Z. Guan, "Beam learning in mmwave/thz-band drone networks under in-flight mobility uncertainties," *IEEE Transactions on Mobile Computing*, 2020.
- [22] P. K. Gkonis, P. T. Trakadas, and D. I. Kaklamani, "A comprehensive study on simulation techniques for 5g networks: State of the art results, analysis, and future challenges," *Electronics*, vol. 9, no. 3, p. 468, 2020.
- [23] V. Begishev, A. Samuylov, D. Moltchanov, E. Machnev, Y. Koucheryavy, and K. Samouylov, "Connectivity properties of vehicles in street deployment of 3gpp nr systems," in *2018 IEEE Globecom Workshops (GC Wkshps)*. IEEE, 2018, pp. 1–7.
- [24] M. Gapeyenko, A. Samuylov, M. Gerasimenko, D. Moltchanov, S. Singh, M. R. Akdeniz, E. Aryafar, N. Himayat, S. Andreev, and Y. Koucheryavy, "On the temporal effects of mobile blockers in urban millimeter-wave cellular scenarios," *IEEE Transactions on Vehicular Technology*, available online, 2017.
- [25] Y. Yaman and P. Spasojevic, "A ray tracing intra-cluster model with diffuse scattering for mmwave communications," *IEEE Antennas and Wireless Propagation Letters*, 2021.
- [26] D. Solomitckii, "Evaluation of mmwave 5g performance by advanced ray tracing techniques," 2019.
- [27] M. Lecci, P. Testolina, M. Polese, M. Giordani, and M. Zorzi, "Accuracy vs. complexity for mmwave ray-tracing: A full stack perspective," *arXiv preprint arXiv:2007.07125*, 2020.
- [28] M. Lecci, P. Testolina, M. Giordani, M. Polese, T. Ropitault, C. Gentile, N. Varshney, A. Bodi, and M. Zorzi, "Simplified ray tracing for the millimeter wave channel: a performance evaluation," in *2020 Information Theory and Applications Workshop (ITA)*. IEEE, 2020, pp. 1–6.
- [29] H. ElSawy, A. Sultan-Salem, M.-S. Alouini, and M. Z. Win, "Modeling and analysis of cellular networks using stochastic geometry: A tutorial," *IEEE Communications Surveys & Tutorials*, vol. 19, no. 1, pp. 167–203, 2016.
- [30] H. ElSawy, E. Hossain, and M. Haenggi, "Stochastic geometry for modeling, analysis, and design of multi-tier and cognitive cellular wireless networks: A survey," *IEEE Communications Surveys & Tutorials*, vol. 15, no. 3, pp. 996–1019, 2013.
- [31] M. Haenggi, *Stochastic geometry for wireless networks*. Cambridge University Press, 2012.
- [32] M. Haenggi, J. G. Andrews, F. Baccelli, O. Dousse, and M. Franceschetti, "Stochastic geometry and random graphs for the analysis and design of wireless networks," *IEEE journal on selected areas in communications*, vol. 27, no. 7, pp. 1029–1046, 2009.
- [33] B. Błaszczyszyn, M. Haenggi, P. Keeler, and S. Mukherjee, *Stochastic geometry analysis of cellular networks*. Cambridge University Press, 2018.
- [34] R. Vannithamby and S. Talwar, *Towards 5G: Applications, requirements and candidate technologies*. John Wiley & Sons, 2017.
- [35] L. Bariah, L. Mohjazi, S. Muhaidat, P. C. Sofotasios, G. K. Kurt, H. Yanikomeroglu, and O. A. Dobre, "A prospective look: Key enabling technologies, applications and open research topics in 6G networks," *IEEE Access*, vol. 8, pp. 174 792–174 820, 2020.
- [36] A. Ghosh, R. Ratasuk, and F. Vook, "Nr radio interface for 5g verticals," *5G Verticals: Customizing Applications, Technologies and Deployment Techniques*, pp. 57–91, 2020.
- [37] J. Kokkonen, J. Lehtomäki, V. Petrov, D. Moltchanov, and M. Juntti, "Frequency domain penetration loss in the terahertz band," in *2016 Global Symposium on Millimeter Waves (GSMM) & ESA Workshop on Millimeter-Wave Technology and Applications*. IEEE, 2016, pp. 1–4.
- [38] 3GPP, "Study on channel model for frequencies from 0.5 to 100 GHz (Release 14)," 3GPP TR 38.901 V14.1.1, July 2017.
- [39] M. Gapeyenko, A. Samuylov, M. Gerasimenko, D. Moltchanov, S. Singh, M. R. Akdeniz, E. Aryafar, S. Andreev, N. Himayat, and Y. Koucheryavy, "Spatially-consistent human body blockage modeling: a state generation procedure," *IEEE Transactions on Mobile Computing*, vol. 9, no. 17, p. 20, 2019.
- [40] M. Gapeyenko, A. Samuylov, M. Gerasimenko, D. Moltchanov, S. Singh, E. Aryafar, S.-p. Yeh, N. Himayat, S. Andreev, and Y. Koucheryavy, "Analysis of human-body blockage in urban millimeter-wave cellular communications," in *Communications (ICC), 2016 IEEE International Conference on*. IEEE, 2016, pp. 1–7.
- [41] E. Björnson, L. Sanguinetti, H. Wymeersch, J. Hoydis, and T. L. Marzetta, "Massive mimo is a reality – what is next?: Five promising research directions for antenna arrays," *Digital Signal Processing*, vol. 94, pp. 3–20, 2019.
- [42] E. Ali, M. Ismail, R. Nordin, and N. F. Abdulah, "Beamforming techniques for massive mimo systems in 5g: overview, classification, and trends for future research," *Frontiers of Information Technology & Electronic Engineering*, vol. 18, no. 6, pp. 753–772, 2017.
- [43] A. Singh, M. Andrello, N. Thawdar, and J. M. Jornet, "Design and operation of a graphene-based plasmonic nano-antenna array for communication in the terahertz band," *IEEE Journal on Selected Areas in Communications*, vol. 38, no. 9, pp. 2104–2117, 2020.
- [44] C. Han, L. Yan, and J. Yuan, "Hybrid beamforming for terahertz wireless communications: Challenges, architectures, and open problems," *arXiv preprint arXiv:2101.08469*, 2021.
- [45] V. Petrov, M. Komarov, D. Moltchanov, J. M. Jornet, and Y. Koucheryavy, "Interference and sinr in millimeter wave and terahertz communication systems with blocking and directional antennas," *IEEE Transactions on Wireless Communications*, vol. 16, no. 3, pp. 1791–1808, 2017.
- [46] S. Hur *et al.*, "Millimeter wave beamforming for wireless backhaul and access in small cell networks," *IEEE Trans. on Commun.*, vol. 61, no. 10, pp. 4391–4403, Oct. 2013.
- [47] J. Kokkonen, A.-A. A. Boulogeorgos, M. Aminu, J. Lehtomäki, A. Alexiou, and M. Juntti, "Impact of beam misalignment on thz wireless systems," *Nano Communication Networks*, p. 100302, 2020.
- [48] B. Peng and T. Kurner, "Three-dimensional angle of arrival estimation in dynamic indoor terahertz channels using a forward-backward algorithm," *IEEE Trans. on Vehic. Tech.*, vol. 66, no. 5, pp. 3798–3811, May 2017.
- [49] F. Hu, Y. Deng, H. Zhou, T. H. Jung, C.-B. Chae, and A. H. Aghvami, "A vision of an xr-aided teleoperation system toward 5g/b5g," *IEEE Communications Magazine*, vol. 59, no. 1, pp. 34–40, 2021.
- [50] 3GPP, "NR; Multi-connectivity; stage 2 (Release 16)," 3GPP TS 37.340 V16.0.0, December 2019.
- [51] H. Holma, A. Toskala, and T. Nakamura, *5G Technology: 3GPP New Radio*. John Wiley & Sons, 2020.
- [52] V. Raghavan, V. Podshivalov, J. Hulten, M. A. Tassoudji, A. Sampath, O. H. Koymen, and J. Li, "Spatio-temporal impact of hand and body blockage for millimeter-wave user equipment design at 28 ghz," *IEEE Communications Magazine*, vol. 56, no. 12, pp. 46–52, 2021.
- [53] D. Moltchanov, A. Samuylov, V. Petrov, M. Gapeyenko, N. Himayat, S. Andreev, and Y. Koucheryavy, "Improving session continuity with bandwidth reservation in mmwave communications," *IEEE Wireless Communications Letters*, vol. 8, no. 1, pp. 105–108, 2018.
- [54] V. Begishev, E. Sopin, D. Moltchanov, R. Kovalchukov, A. Samuylov, S. Andreev, Y. Koucheryavy, and K. Samouylov, "Joint use of guard capacity and multiconnectivity for improved session continuity in millimeter-wave 5g nr systems," *IEEE Transactions on Vehicular Technology*, 2021.
- [55] E. Dahlman, S. Parkvall, and J. Skold, *5G NR: The next generation wireless access technology*. Academic Press, 2020.
- [56] A. Samuylov, D. Moltchanov, R. Kovalchukov, R. Pirmagomedov, Y. Gaidamaka, S. Andreev, Y. Koucheryavy, and K. Samouylov, "Characterizing resource allocation trade-offs in 5g nr serving multicast and unicast traffic," *IEEE Transactions on Wireless Communications*, vol. 19, no. 5, pp. 3421–3434, 2020.
- [57] V. Begishev, D. Moltchanov, E. Sopin, A. Samuylov, S. Andreev, Y. Koucheryavy, and K. Samouylov, "Quantifying the impact of guard capacity on session continuity in 3gpp new radio systems," *IEEE Transactions on Vehicular Technology*, vol. 68, no. 12, pp. 12 345–12 359, 2019.
- [58] N. H. Mahmood, M. Lopez, D. Laselva, K. Pedersen, and G. Berardinelli, "Reliability oriented dual connectivity for URLLC services in 5G New Radio," in *2018 15th International Symposium on Wireless Communication Systems (ISWCS)*. IEEE, 2018, pp. 1–6.
- [59] J. Rao and S. Vrzic, "Packet duplication for URLLC in 5G: Architectural enhancements and performance analysis," *IEEE Network*, vol. 32, no. 2, pp. 32–40, 2018.
- [60] N. H. Mahmood, A. Karimi, G. Berardinelli, K. I. Pedersen, and D. Laselva, "On the resource utilization of multi-connectivity transmission for URLLC services in 5G New Radio," in *2019 IEEE Wireless*

- Communications and Networking Conference Workshop (WCNCW)*. IEEE, 2019, pp. 1–6.
- [61] A. Anand et al., “Joint scheduling of urllc and embb traffic in 5g wireless networks,” *IEEE/ACM Transactions on Networking*, 2020.
- [62] R. Kassab et al., “Coexistence of URLLC and eMBB services in the C-RAN uplink: an information-theoretic study,” in *2018 IEEE Global Communications Conference (GLOBECOM)*. IEEE, 2018, pp. 1–6.
- [63] S. Doğan, A. Tusha, and H. Arslan, “Noma with index modulation for uplink urllc through grant-free access,” *IEEE Journal of Selected Topics in Signal Processing*, vol. 13, no. 6, pp. 1249–1257, 2019.
- [64] R. Kotaba, C. N. Manchón, T. Balercia, and P. Popovski, “How urllc can benefit from noma-based retransmissions,” *IEEE Transactions on Wireless Communications*, 2020.
- [65] O. Sallent, J. Perez-Romero, R. Ferrus, and R. Agustí, “On radio access network slicing from a radio resource management perspective,” *IEEE Wireless Communications*, vol. 24, no. 5, pp. 166–174, 2017.
- [66] P. Popovski, K. F. Trillingsgaard, O. Simeone, and G. Durisi, “5G wireless network slicing for eMBB, URLLC, and mMTC: A communication-theoretic view,” *IEEE Access*, vol. 6, pp. 55 765–55 779, 2018.
- [67] Y. Koucheryavy, E. Lisovskaya, D. Moltchanov, R. Kovalchukov, and A. Samuylov, “Quantifying the millimeter wave new radio base stations density for network slicing with prescribed slas,” *Computer Communications*, 2021.
- [68] E. Markova, D. Moltchanov, R. Pirmagomedov, D. Ivanova, Y. Koucheryavy, and K. Samouylov, “Prioritized service of urllc traffic in industrial deployments of 5g nr systems,” in *International Conference on Distributed Computer and Communication Networks*. Springer, 2020, pp. 497–509.
- [69] E. Markoval, D. Moltchanov, R. Pirmagomedov, D. Ivanova, Y. Koucheryavy, and K. Samouylov, “Priority-based coexistence of embb and urllc traffic in industrial 5g nr deployments,” in *2020 12th International Congress on Ultra Modern Telecommunications and Control Systems and Workshops (ICUMT)*. IEEE, 2020, pp. 1–6.
- [70] T. Maksymyuk, M. Brych, and V. Pelishok, “Stochastic geometry models for 5g heterogeneous mobile networks,” *SmartCR*, vol. 5, no. 2, pp. 89–101, 2015.
- [71] M. Di Renzo, “Stochastic geometry modeling and analysis of multi-tier millimeter wave cellular networks,” *IEEE Transactions on Wireless Communications*, vol. 14, no. 9, pp. 5038–5057, 2015.
- [72] D. Moltchanov, “Distance distributions in random networks,” *Ad Hoc Networks*, vol. 10, no. 6, pp. 1146–1166, 2012.
- [73] Y. Li, F. Baccelli, H. S. Dhillon, and J. G. Andrews, “Statistical modeling and probabilistic analysis of cellular networks with determinantal point processes,” *IEEE Transactions on Communications*, vol. 63, no. 9, pp. 3405–3422, 2015.
- [74] R. Kovalchukov, D. Moltchanov, A. Samuylov, A. Ometov, S. Andreev, Y. Koucheryavy, and K. Samouylov, “Analyzing effects of directionality and random heights in drone-based mmwave communication,” *IEEE Transactions on Vehicular Technology*, vol. 67, no. 10, pp. 10064–10069, 2018.
- [75] —, “Evaluating SIR in 3D millimeter-wave deployments: Direct modeling and feasible approximations,” *IEEE Transactions on Wireless Communications*, vol. 18, no. 2, pp. 879–896, 2019.
- [76] W. Yi, Y. Liu, E. Bodanese, A. Nallanathan, and G. K. Karagiannidis, “A unified spatial framework for uav-aided mmwave networks,” *IEEE Transactions on Communications*, vol. 67, no. 12, pp. 8801–8817, 2019.
- [77] W. Yi, Y. Liu, Y. Deng, and A. Nallanathan, “Clustered uav networks with millimeter wave communications: A stochastic geometry view,” *IEEE Transactions on Communications*, vol. 68, no. 7, pp. 4342–4357, 2020.
- [78] D. He, L. Wang, K. Guan, B. Ai, J. Kim, and Z. Zhong, “Channel characterization for mmwave vehicle-to-infrastructure communications in urban street environment,” in *2019 13th European Conference on Antennas and Propagation (EuCAP)*. IEEE, 2019, pp. 1–5.
- [79] M. S. Kumari, N. Kumar, and R. Prasad, “Optimization of street canyon outdoor channel deployment geometry for mmwave 5g communication,” *AEU-International Journal of Electronics and Communications*, vol. 125, p. 153368, 2020.
- [80] M. Boban, D. Dupleich, N. Iqbal, J. Luo, C. Schneider, R. Müller, Z. Yu, D. Steer, T. Jämsä, J. Li et al., “Multi-band vehicle-to-vehicle channel characterization in the presence of vehicle blockage,” *IEEE Access*, vol. 7, pp. 9724–9735, 2019.
- [81] J.-J. Park, J. Lee, J. Liang, K.-W. Kim, K.-C. Lee, and M.-D. Kim, “Millimeter wave vehicular blockage characteristics based on 28 GHz measurements,” in *Proc. of IEEE 86th Vehicular Technology Conference (IEEE VTC-Fall)*, 2017, pp. 1–5.
- [82] V. Petrov, J. M. Eckhardt, D. Moltchanov, Y. Koucheryavy, and T. Kurner, “Measurements of reflection and penetration losses in low terahertz band vehicular communications,” in *2020 14th European Conference on Antennas and Propagation*. IEEE, 2020, pp. 1–5.
- [83] J. Eckhardt, V. Petrov, Moltchanov, Y. Koucheryavy, and T. Kurner, “Channel measurements and modeling for low terahertz band vehicular communications,” *IEEE Journal on Selected Areas in Communications*, 2021.
- [84] R. Kovalchukov, D. Moltchanov, V. Begishev, A. Samuylov, S. Andreev, Y. Koucheryavy, and K. Samouylov, “Improved session continuity in 5g nr with joint use of multi-connectivity and guard bandwidth,” in *2018 IEEE Global Communications Conference (GLOBECOM)*. IEEE, 2018, pp. 1–7.
- [85] Y. Chen, Y. Li, C. Han, Z. Yu, and G. Wang, “Channel measurement and ray-tracing-statistical hybrid modeling for low-terahertz indoor communications,” *arXiv preprint arXiv:2101.12436*, 2021.
- [86] Y. Xing, T. S. Rappaport, and A. Ghosh, “Millimeter wave and sub-thz indoor radio propagation channel measurements, models, and comparisons in an office environment,” *arXiv preprint arXiv:2103.00385*, 2021.
- [87] V. Petrov, D. Moltchanov, S. Andreev, and R. W. Heath, “Analysis of intelligent vehicular relaying in urban 5g+ millimeter-wave cellular deployments,” in *2019 IEEE Global Communications Conference (GLOBECOM)*. IEEE, 2019, pp. 1–6.
- [88] Y. Wang, K. Venugopal, A. F. Molisch, and R. W. Heath, “Blockage and coverage analysis with mmwave cross street bss near urban intersections,” in *2017 IEEE International Conference on Communications (ICC)*. IEEE, 2017, pp. 1–6.
- [89] —, “Mmwave vehicle-to-infrastructure communication: Analysis of urban microcellular networks,” *IEEE Transactions on Vehicular Technology*, vol. 67, no. 8, pp. 7086–7100, 2018.
- [90] 3GPP, “Study on channel model for frequencies from 0.5 to 100 GHz (Release 14),” 3GPP TR 38.901 V14.1.1, July 2017.
- [91] Y. Xing and T. S. Rappaport, “Propagation measurements and path loss models for sub-thz in urban microcells,” *arXiv preprint arXiv:2103.01151*, 2021.
- [92] J. M. Jornet and I. F. Akyildiz, “Channel modeling and capacity analysis for electromagnetic wireless nanonetworks in the terahertz band,” *IEEE Transactions on Wireless Communications*, vol. 10, no. 10, pp. 3211–3221, 2011.
- [93] —, “Femtosecond-long pulse-based modulation for terahertz band communication in nanonetworks,” *IEEE Transactions on Communications*, vol. 62, no. 5, pp. 1742–1754, 2014.
- [94] L. S. Rothman et al., “HITRAN: High-resolution transmission molecular absorption database,” Harvard-Smithson Center for Astrophysics, www.cfa.harvard.edu, 2014.
- [95] P. Boronin, V. Petrov, D. Moltchanov, Y. Koucheryavy, and J. M. Jornet, “Capacity and throughput analysis of nanoscale machine communication through transparency windows in the terahertz band,” *Nano Communication Networks*, vol. 5, no. 3, pp. 72–82, 2014.
- [96] P. Boronin, D. Moltchanov, and Y. Koucheryavy, “A molecular noise model for thz channels,” in *2015 IEEE International Conference on Communications (ICC)*. IEEE, 2015, pp. 1286–1291.
- [97] J. Kokkonen, J. Lehtomäki, and M. Juntti, “A discussion on molecular absorption noise in the terahertz band,” *Nano communication networks*, vol. 8, pp. 35–45, 2016.
- [98] 3GPP, “Study on 3D channel model for LTE,” *TR 36.873 V12.2.0*, 2015.
- [99] M. Gapeyenko, V. Petrov, D. Moltchanov, S. Andreev, Y. Koucheryavy, M. Valkama, M. R. Akdeniz, and N. Himayat, “An analytical representation of the 3gpp 3d channel model parameters for mmwave bands,” in *Proceedings of the 2nd ACM Workshop on Millimeter Wave Networks and Sensing Systems*. ACM, 2018, pp. 33–38.
- [100] R. He, C. Schneider, B. Ai, G. Wang, Z. Zhong, D. A. Dupleich, R. S. Thomae, M. Boban, J. Luo, and Y. Zhang, “Propagation channels of 5g millimeter-wave vehicle-to-vehicle communications: Recent advances and future challenges,” *IEEE vehicular technology magazine*, vol. 15, no. 1, pp. 16–26, 2019.
- [101] K. Guan, B. Peng, D. He, J. M. Eckhardt, S. Rey, B. Ai, Z. Zhong, and T. Kürner, “Measurement, simulation, and characterization of train-to-infrastructure inside-station channel at the terahertz band,” *IEEE Transactions on Terahertz Science and Technology*, vol. 9, no. 3, pp. 291–306, 2019.
- [102] D. He, K. Guan, A. Fricke, B. Ai, R. He, Z. Zhong, A. Kasamatsu, I. Hosako, and T. Kürner, “Stochastic channel modeling for kiosk

- applications in the terahertz band," *IEEE Transactions on Terahertz Science and Technology*, vol. 7, no. 5, pp. 502–513, 2017.
- [103] A. Ometov, D. Moltchanov, M. Komarov, S. V. Volvenko, and Y. Koucheryavy, "Packet level performance assessment of mmwave backhauling technology for 3gpp nr systems," *IEEE Access*, vol. 7, pp. 9860–9871, 2019.
- [104] S. Sun, G. R. MacCartney, and T. S. Rappaport, "A novel millimeter-wave channel simulator and applications for 5G wireless communications," in *Proc. of International Conference on Communications (ICC)*. IEEE, 2017, pp. 1–7.
- [105] A. Ghosh, T. A. Thomas, M. C. Cudak, R. Ratasuk, P. Moorut, F. W. Vook, T. S. Rappaport, G. R. MacCartney, S. Sun, and S. Nie, "Millimeter-wave enhanced local area systems: A high-data-rate approach for future wireless networks," *IEEE Journal on Selected Areas in Communications*, vol. 32, no. 6, pp. 1152–1163, 2014.
- [106] F. Khan and Z. Pi, "mmWave mobile broadband (MMB): Unleashing the 3–300GHz spectrum," in *Proc. of 34th Sarnoff Symposium*. IEEE, 2011, pp. 1–6.
- [107] T. L. Frey, "The Effects of the Atmosphere and Weather on the Performance of a mm-Wave Communication Link," *Applied Microwave and Wireless*, vol. 11, pp. 76–81, 1999.
- [108] H. J. Liebe, T. Manabe, and G. A. Hufford, "Millimeter-wave attenuation and delay rates due to fog/cloud conditions," *IEEE Transactions on Antennas and Propagation*, vol. 37, no. 12, pp. 1617–1612, 1989.
- [109] A. Foessel, S. Chheda, and D. Apostolopoulos, "Short-range millimeter-wave radar perception in a polar environment," 1999.
- [110] A. Y. Nashashibi, K. Sarabandi, S. Oveisgharan, M. C. Dobson, W. S. Walker, and E. Burke, "Millimeter-wave measurements of foliage attenuation and ground reflectivity of tree stands at nadir incidence," *IEEE Transactions on Antennas and Propagation*, vol. 52, no. 5, pp. 1211–1222, 2004.
- [111] F. K. Scherwing, E. J. Violette, and R. H. Espeland, "Millimeter-wave propagation in vegetation: Experiments and theory," *IEEE Transactions on Geoscience and Remote Sensing*, vol. 26, no. 3, pp. 355–367, 1988.
- [112] C. Slezak, V. Semkin, S. Andreev, Y. Koucheryavy, and S. Rangan, "Empirical effects of dynamic human-body blockage in 60 ghz communications," *IEEE Communications Magazine*, vol. 56, no. 12, pp. 60–66, 2018.
- [113] R. J. Weiler, M. Peter, W. Keusgen, K. Sakaguchi, and F. Undi, "Environment induced shadowing of urban millimeter-wave access links," *IEEE Wireless Communications Letters*, vol. 5, no. 4, pp. 440–443, 2016.
- [114] G. R. MacCartney, T. S. Rappaport, and S. Rangan, "Rapid fading due to human blockage in pedestrian crowds at 5g millimeter-wave frequencies," in *GLOBECOM 2017-2017 IEEE Global Communications Conference*. IEEE, 2017, pp. 1–7.
- [115] B. A. Bilgin, H. Ramezani, and O. B. Akan, "Human blockage model for indoor terahertz band communication," in *2019 IEEE International Conference on Communications Workshops (ICC Workshops)*. IEEE, 2019, pp. 1–6.
- [116] A. Yamamoto, K. Ogawa, T. Horimatsu, A. Kato, and M. Fujise, "Path-loss prediction models for intervehicle communication at 60 GHz," *IEEE Transactions on Vehicular Technology*, vol. 57, no. 1, pp. 65–78, January 2008.
- [117] J.-J. Park, J. Lee, K.-W. Kim, K.-C. Lee, and M.-D. Kim, "Vehicle antenna position dependent path loss for millimeter-wave V2V communication," in *Proc. of 11th Global Symposium on Millimeter Waves (GSMM)*, May 2018, pp. 1–3.
- [118] T. Bai, R. Vaze, and R. W. Heath, "Analysis of blockage effects on urban cellular networks," *IEEE Transactions on Wireless Communications*, vol. 13, no. 9, pp. 5070–5083, September 2014.
- [119] A. Samuylov, M. Gapeyenko, D. Moltchanov, M. Gerasimenko, S. Singh, N. Himayat, S. Andreev, and Y. Koucheryavy, "Characterizing spatial correlation of blockage statistics in urban mmwave systems," in *IEEE Globecom Workshops (GC Wkshps)*, December 2016, pp. 1–7.
- [120] P. Nain, D. Towsley, B. Liu, and Z. Liu, "Properties of random direction models," in *IEEE 24th Annual Joint Conference of the IEEE Computer and Communications Societies*, vol. 3, March 2005, pp. 1897–1907.
- [121] D. J. Daley and L. Servi, "Idle and busy periods in stable M/M/k queues," *Journal of applied probability*, vol. 35, no. 4, pp. 950–962, 1998.
- [122] D. Moltchanov, A. Ometov, and Y. Koucheryavy, "Analytical characterization of the blockage process in 3gpp new radio systems with trilateral mobility and multi-connectivity," *Computer Communications*, vol. 146, pp. 110–120, 2019.
- [123] G. R. MacCartney, T. S. Rappaport, and A. Ghosh, "Base Station Diversity Propagation Measurements at 73 GHz Millimeter-Wave for 5G Coordinated Multipoint (CoMP) Analysis," in *IEEE Global Communications Workshops (GLOBECOM Wkshps)*, December 2017, pp. 1–7.
- [124] S. Aditya, H. S. Dhillon, A. F. Molisch, and H. Behairy, "A tractable analysis of the blind-spot probability in localization networks under correlated blocking," Available: <https://arxiv.org/pdf/1801.08560.pdf>, pp. 1–30, January 2018.
- [125] T. Bai, R. Vaze, and R. W. Heath Jr., "Analysis of blockage effects on urban cellular networks," *IEEE Transactions on Wireless Communications*, vol. 13, no. 9, pp. 5070–5083, September 2014.
- [126] M. Gapeyenko, D. Moltchanov, S. Andreev, and R. Heath, "Line-of-Sight Probability for mmWave-based UAV Communications in Regular 3D City Deployments," *IEEE Transactions on Wireless Communications*, vol. X, no. X, pp. xxxx–xxxx, Xxx 2021.
- [127] F. Baccelli and X. Zhang, "A correlated shadowing model for urban wireless networks," in *2015 IEEE Conference on Computer Communications (INFOCOM)*, April 2015, pp. 801–809.
- [128] T. Bai and R. W. Heath, "Coverage and rate analysis for millimeter-wave cellular networks," *IEEE Transactions on Wireless Communications*, vol. 14, no. 2, pp. 1100–1114, February 2015.
- [129] M. Gapeyenko, V. Petrov, D. Moltchanov, M. R. Akdeniz, S. Andreev, N. Himayat, and Y. Koucheryavy, "On the degree of multi-connectivity in 5g millimeter-wave cellular urban deployments," *IEEE Transactions on Vehicular Technology*, vol. 68, no. 2, pp. 1973–1978, 2019.
- [130] S. Singh, R. Mudumbai, and U. Madhow, "Interference analysis for highly directional 60-ghz mesh networks: The case for rethinking medium access control," *IEEE/ACM Transactions on Networking (TON)*, vol. 19, no. 5, pp. 1513–1527, 2011.
- [131] H. Park, S. Park, T. Song, and S. Pack, "An incremental multicast grouping scheme for mmwave networks with directional antennas," *IEEE Communications Letters*, vol. 17, no. 3, pp. 616–619, 2013.
- [132] V. Petrov, M. Komarov, D. Moltchanov, J. M. Jornet, and Y. Koucheryavy, "Interference analysis of EHF/THF communications systems with blocking and directional antennas," in *Global Communications Conference (GLOBECOM)*. IEEE, 2016, pp. 1–7.
- [133] A. Biazon and M. Zorzi, "Multicast via point to multipoint transmissions in directional 5g mmwave communications," *IEEE Communications Magazine*, vol. 57, no. 2, pp. 88–94, 2019.
- [134] H. Zhang, Y. Jiang, K. Sundaresan, S. Rangarajan, and B. Zhao, "Wireless Multicast Scheduling with Switched Beamforming Antennas," *IEEE/ACM Transactions on Networking*, vol. 20, no. 5, pp. 1595–1607, 2012.
- [135] M. Petrera and Y. B. Suris, "Spherical geometry and integrable systems," *Geometriae Dedicata*, vol. 169, no. 1, pp. 83–98, Apr 2014. [Online]. Available: <https://doi.org/10.1007/s10711-013-9843-4>
- [136] A. B. Constantine *et al.*, "Antenna theory: analysis and design," *Microstrip Antennas*, John Wiley & Sons, 2005.
- [137] M. Gerasimenko, D. Moltchanov, M. Gapeyenko, S. Andreev, and Y. Koucheryavy, "Capacity of multi-connectivity mmwave systems with dynamic blockage and directional antennas," *IEEE Transactions on Vehicular Technology*, 2019.
- [138] D. Piazza, N. J. Kirsch, A. Forenza, R. W. Heath, and K. R. Dandekar, "Design and evaluation of a reconfigurable antenna array for mimo systems," *IEEE Transactions on antennas and propagation*, vol. 56, no. 3, pp. 869–881, 2008.
- [139] H.-T. Kim, B.-S. Park, S.-S. Song, T.-S. Moon, S.-H. Kim, J.-M. Kim, J.-Y. Chang, and Y.-C. Ho, "A 28-ghz cmos direct conversion transceiver with packaged 2x4 antenna array for 5g cellular system," *IEEE Journal of Solid-State Circuits*, vol. 53, no. 5, pp. 1245–1259, 2018.
- [140] "Telecommunications and information exchange between systems local and metropolitan area networks – specific requirements. Part 11. Amendment 3," IEEE Standard for Information technology, 2012.
- [141] L. Wei, Q. Li, and G. Wu, "Exhaustive, iterative and hybrid initial access techniques in mmwave communications," in *2017 IEEE Wireless Communications and Networking Conference (WCNC)*. IEEE, 2017, pp. 1–6.
- [142] V. Va, H. Vikalo, and R. W. Heath, "Beam tracking for mobile millimeter wave communication systems," in *2016 IEEE Global Conference on Signal and Information Processing (GlobalSIP)*. IEEE, 2016, pp. 743–747.
- [143] J. Lim, H.-M. Park, and D. Hong, "Beam tracking under highly nonlinear mobile millimeter-wave channel," *IEEE Communications Letters*, vol. 23, no. 3, pp. 450–453, 2019.
- [144] D.-S. Shim, C.-K. Yang, J. H. Kim, J. P. Han, and Y. S. Cho, "Application of motion sensors for beam-tracking of mobile stations

- in mmwave communication systems,” *Sensors*, vol. 14, no. 10, pp. 19 622–19 638, 2014.
- [145] M. Alrabeiah, J. Booth, A. Hredzak, and A. Alkhateeb, “Viwi vision-aided mmwave beam tracking: Dataset, task, and baseline solutions,” *arXiv preprint arXiv:2002.02445*, 2020.
- [146] M. Brambilla, D. Tagliaferri, M. Nicoli, and U. Spagnolini, “Sensor and map-aided cooperative beam tracking for optical v2v communications,” in *2020 IEEE 91st Vehicular Technology Conference (VTC2020-Spring)*. IEEE, 2020, pp. 1–7.
- [147] V. Petrov, G. Fodor, J. Kokkonen, D. Moltchanov, J. Lehtomaki, S. Andreev, Y. Koucheryavy, M. Juntti, and M. Valkama, “On unified vehicular communications and radar sensing in millimeter-wave and low terahertz bands,” *IEEE wireless communications*, vol. 26, no. 3, pp. 146–153, 2019.
- [148] J. Gui, Y. Liu, X. Deng, and B. Liu, “Network capacity optimization for cellular-assisted vehicular systems by online learning-based mmwave beam selection,” *Wireless Communications and Mobile Computing*, vol. 2021, 2021.
- [149] C. Liu, M. Li, S. V. Hanly, P. Whiting, and I. B. Collings, “Millimeter-wave small cells: Base station discovery, beam alignment, and system design challenges,” *IEEE Wireless Communications*, vol. 25, no. 4, pp. 40–46, 2018.
- [150] S. Kutty and D. Sen, “Beamforming for millimeter wave communications: An inclusive survey,” *IEEE Communications Surveys & Tutorials*, vol. 18, no. 2, pp. 949–973, 2015.
- [151] I. Aykin, B. Akgun, M. Feng, and M. Krunz, “Mamba: A multi-armed bandit framework for beam tracking in millimeter-wave systems,” in *IEEE INFOCOM 2020-IEEE Conference on Computer Communications*. IEEE, 2020, pp. 1469–1478.
- [152] J. Jeong, S. H. Lim, Y. Song, and S.-W. Jeon, “Online learning for joint beam tracking and pattern optimization in massive mimo systems,” in *IEEE INFOCOM 2020-IEEE Conference on Computer Communications*. IEEE, 2020, pp. 764–773.
- [153] 3GPP, “NR; Physical channels and modulation (Release 15),” 3GPP TR 38.211, Dec 2017.
- [154] V. Begishev, E. Sopin, D. Moltchanov, R. Pirmagomedov, A. Samuylov, S. Andreev, Y. Koucheryavy, and K. Samouylov, “Performance Analysis of Multi-Band Microwave and Millimeter-Wave Operation in 5G NR Systems,” *IEEE Transactions on Wireless Communications*, vol. X, no. X, pp. xxxx–xxxx, Xxx 2021.
- [155] A. V. Gorbunova, V. A. Naumov, Y. V. Gaidamaka, and K. E. Samouylov, “Resource queuing systems as models of wireless communication systems,” *Informatika i ee Primeneniya*, vol. 12, no. 3, pp. 48–55, 2018.
- [156] —, “Resource queuing systems with general service discipline,” *Informatika i ee Primeneniya*, vol. 13, no. 1, pp. 99–107, 2019.
- [157] V. A. Naumov, K. E. Samouylov, and A. K. Samouylov, “On the total amount of resources occupied by serviced customers,” *Automation and Remote Control*, vol. 77, no. 8, pp. 1419–1427, 2016.
- [158] A. Bobbio and K. S. Trivedi, “An aggregation technique for the transient analysis of stiff markov chains,” *IEEE Transactions on computers*, no. 9, pp. 803–814, 1986.
- [159] G. Ciardo and E. Smirni, “Etaqa: an efficient technique for the analysis of qbd-processes by aggregation,” *Performance Evaluation*, vol. 36, pp. 71–93, 1999.
- [160] K. Samouylov, E. Sopin, and O. Vikhrova, “Analyzing blocking probability in lte wireless network via queuing system with finite amount of resources,” in *Information Technologies and Mathematical Modelling - Queueing Theory and Applications*. Cham: Springer International Publishing, 2015, pp. 393–403.
- [161] E. Sopin, K. Ageev, E. Markova, O. Vikhrova, and Y. Gaidamaka, “Performance analysis of m2m traffic in lte network using queuing systems with random resource requirements,” *Automatic Control and Computer Sciences*, vol. 52, pp. 345–353, 2018.
- [162] N. Seitz, “ITU-T QoS standards for IP-based networks,” *IEEE Communications Magazine*, vol. 41, no. 6, pp. 82–89, 2003.
- [163] R. Serral-Gracià, E. Cerqueira, M. Curado, M. Yannuzzi, E. Monteiro, and X. Masip-Bruin, “An overview of quality of experience measurement challenges for video applications in ip networks,” in *International Conference on Wired/Wireless Internet Communications*. Springer, 2010, pp. 252–263.
- [164] T. De Pessemier, K. De Moor, W. Joseph, L. De Marez, and L. Martens, “Quantifying the influence of rebuffering interruptions on the user’s quality of experience during mobile video watching,” *IEEE Transactions on Broadcasting*, vol. 59, no. 1, pp. 47–61, 2012.
- [165] F. Dobrian, V. Sekar, A. Awan, I. Stoica, D. Joseph, A. Ganjam, J. Zhan, and H. Zhang, “Understanding the impact of video quality on user engagement,” *ACM SIGCOMM Computer Communication Review*, vol. 41, no. 4, pp. 362–373, 2011.
- [166] J. Jia and S. S. Heragu, “Solving semi-open queuing networks,” *Operations research*, vol. 57, no. 2, pp. 391–401, 2009.
- [167] P. Kuehn, “Approximate analysis of general queuing networks by decomposition,” *IEEE Transactions on Communications*, vol. 27, no. 1, pp. 113–126, 1979.
- [168] S. B. Gershwin, “An efficient decomposition method for the approximate evaluation of tandem queues with finite storage space and blocking,” *Operations research*, vol. 35, no. 2, pp. 291–305, 1987.
- [169] Q.-M. He, *Fundamentals of matrix-analytic methods*. Springer, 2014, vol. 365.
- [170] G. Latouche and V. Ramaswami, *Introduction to matrix analytic methods in stochastic modeling*. SIAM, 1999.
- [171] E. Sopin, V. Begishev, D. Moltchanov, and A. Samuylov, “Resource queuing system with preemptive priority for performance analysis of 5g nr systems,” in *International Conference on Distributed Computer and Communication Networks*. Springer, 2020, pp. 87–99.
- [172] W. Chen, L. Li, Z. Chen, and T. Quek, “Coverage modelling and analysis for outdoor thz networks with blockage and molecular absorption,” *IEEE Wireless Communications Letters*, 2021.
- [173] A. Shafie, N. Yang, S. Durrani, X. Zhou, C. Han, and M. Juntti, “Coverage analysis for 3d terahertz communication systems,” *IEEE Journal on Selected Areas in Communications*, 2021.
- [174] A. Samuylov, D. Moltchanov, Y. Gaidamaka, S. Andreev, and Y. Koucheryavy, “Random triangle: A baseline model for interference analysis in heterogeneous networks,” *IEEE Transactions on Vehicular Technology*, vol. 65, no. 8, pp. 6778–6782, 2015.
- [175] A. Samuylov, A. Ometov, V. Begishev, R. Kovalchukov, D. Moltchanov, Y. Gaidamaka, K. Samouylov, S. Andreev, and Y. Koucheryavy, “Analytical performance estimation of network-assisted d2d communications in urban scenarios with rectangular cells,” *Transactions on Emerging Technologies*, vol. 28, no. 2, p. e2999, 2017.
- [176] S. N. Chiu, D. Stoyan, W. S. Kendall, and J. Mecke, *Stochastic geometry and its applications*. John Wiley & Sons, 2013.
- [177] 3GPP, “Evolved Universal Terrestrial Radio Access (E-UTRA); Radio Frequency (RF) system scenarios (Release 15),” 3GPP 36.942 V15.0.0, Oct 2018.
- [178] S. Kumar, S. K. Kurtz, J. R. Banavar, and M. Sharma, “Properties of a three-dimensional poisson-voronoi tessellation: A monte carlo study,” *Journal of statistical physics*, vol. 67, no. 3-4, pp. 523–551, 1992.
- [179] M. Tanemura, “Statistical distributions of poisson voronoi cells in two and three dimensions,” *FORMA-TOKYO-*, vol. 18, no. 4, pp. 221–247, 2003.
- [180] S. Ross, *Introduction to probability models*. Academic Press, 2010.
- [181] R. Kovalchukov, D. Moltchanov, Y. Gaidamaka, and E. Bobrikova, “An accurate approximation of resource request distributions in millimeter wave 3gpp new radio systems,” in *Internet of Things, Smart Spaces, and Next Generation Networks and Systems*. Springer, 2019, pp. 572–585.
- [182] R. Groenevelt, “Stochastic models for mobile ad hoc networks,” INRIA Sophia-Antipolis, PhD thesis, 2005.
- [183] J. F. C. Kingman, *Poisson processes*. Wiley Online Library, 1993.
- [184] J. W. Cohen, *The single server queue*. Elsevier, 2012.